iScience

CellPress
OPEN ACCESS

Article

Suppression of ELF4 in ulcerative colitis predisposes host to colorectal cancer

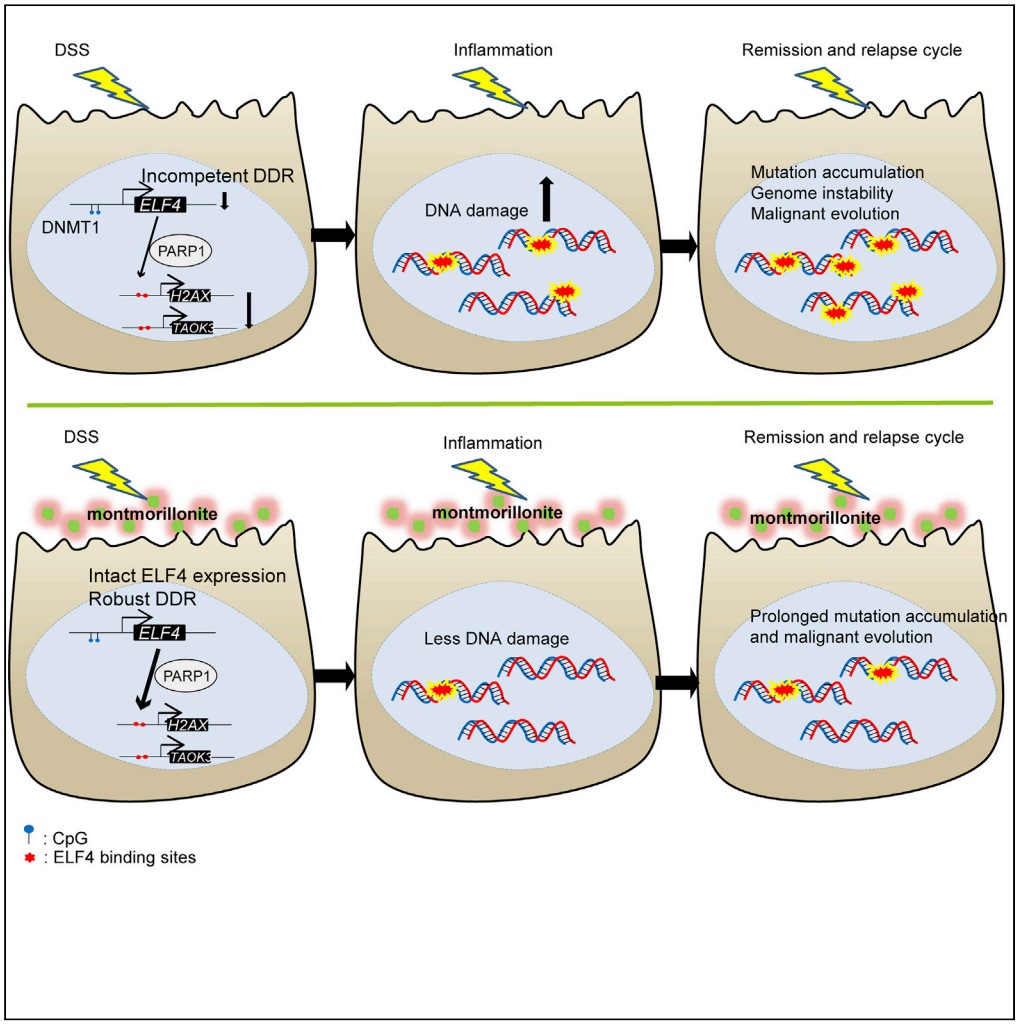

Hongqiang Du, Huawei Xia, Tongtong Liu, ..., Aiwen Wu, Mo Li, Fuping You

drwuaw@sina.com (A.W.)
limo@hsc.pku.edu.cn (M.L.)
fupingyou@hsc.pku.edu.cn (F.Y.)

HIGHLIGHTS

Elf4 expression is suppressed in both colitis and colitis-associated cancer (CAC).

Elf4 deficiency leads to increased hyper-susceptibility to colitis and CAC in mice

Elf4 promotes DNA damage repair upon PARylation by PARP1

Oral administration of montmorillonite lowers risk of CAC development

Du et al., iScience 24, 102169
March 19, 2021
https://doi.org/10.1016/j.isci.2021.102169

iScience

CellPress
OPEN ACCESS

Article

Suppression of ELF4 in ulcerative colitis predisposes host to colorectal cancer

Hongqiang Du,[1,8] Huawei Xia,[1,8] Tongtong Liu,[1,8] Yingjie Li,[2] Jilong Liu,[3] Bingteng Xie,[4,5] Jingxuan Chen,[1] Tong Liu,[6] Lili Cao,[1] Shengde Liu,[1] Siji Li,[1] Peiyan Wang,[1] Dandan Wang,[1] Zeming Zhang,[1] Yunfei Li,[1] Xiaohuan Guo,[7] Aiwen Wu,[2,*] Mo Li,[4,5,*] and Fuping You[1,9,*]

SUMMARY

Ulcerative colitis (UC) is a chronic inflammatory bowel disease, characterized by relapsing and remitting colon mucosal inflammation. For patients suffering from UC, a higher risk of colon cancer has been widely recognized. Here, we found that *Elf4*$^{-/-}$ mice developed colon tumors with 3 cycles of dextran sulfate sodium salt (DSS) treatment alone. We further showed that ELF4 suppression was prevalent in both patients with UC and DSS-induced mice models, and this suppression was caused by promoter region methylation. ELF4, upon PARylation by PARP1, transcriptionally regulated multiple DNA damage repair machinery components. Consistently, ELF4 deficiency leads to more severe DNA damage both *in vitro* and *in vivo*. Oral administration of montmorillonite powder can prevent the reduction of ELF4 in DSS-induced colitis models and lower the risk of colon tumor development during azoxymethane (AOM) and DSS induced colitis-associated cancer (CAC). These data provided additional mechanism of CAC initiation and supported the "epigenetic priming model of tumor initiation".

INTRODUCTION

Ulcerative colitis (UC) is a subtype of inflammatory bowel disease (IBD). Currently, IBD has become a global disease with accelerating incidence in newly industrialized countries whose societies have become more westernized (Ng et al., 2018). UC is characterized by relapsing and remitting colon mucosal inflammation (Ungaro et al., 2017). It has been known for years that patients with UC face a higher risk of colon cancer (Eaden et al., 2001; Jess et al., 2012), namely, colitis-associated cancer (CAC). It should be noted that CAC is different in many ways from sporadic colorectal cancer, namely, CRC (Grivennikov and Cominelli, 2016). CAC serves as an excellent model for studying relation between inflammation and cancer (Grivennikov, 2013).

ELF4 belongs to the E-Twenty-Six (ETS) domain transcription factor family and is involved in a variety of biological processes, including immune response and cell development (Suico et al., 2017). Previously, we have shown that ELF4 is a critical transcription factor for the host antiviral response, during which ELF4 cooperates with nuclear factor-kB (NF-KB) to induce robust interferons and inflammatory cytokine production (You et al., 2013). A recent report indicates that ELF4 is a suppressor of Th17 polarization and plays a role in experimental autoimmune encephalomyelitis (Lee et al., 2014). UC is a chronic inflammatory colon disease with autoimmune roots (Conrad et al., 2014), and whether ELF4 plays a role in the pathogenesis of UC is unknown.

A hallmark of tumor initiation is the presence of genome alterations (Colotta et al., 2009; Fouad and Aanei, 2017). It is long recognized that in addition to direct genotoxic responses, suppression of DNA repair response is also a significant contributor to the accumulated genome alterations during chronic inflammation (Grivennikov, 2013; Sanford et al., 1997), although the mechanism underneath this observation is unknown. Recently, an additional "epigenetic priming" stage of tumor development is proposed (Vicente-Duenas et al., 2018). In this model, epigenetic priming could occur at the very early stage and

[1]Institute of Systems Biomedicine, Department of Immunology, School of Basic Medical Sciences, Beijing Key Laboratory of Tumor Systems Biology, Peking University Health Science Center, Beijing 100000, China

[2]Key Laboratory of Carcinogenesis and Translational Research (Ministry of Education), Department of Gastrointestinal Surgery, Peking University Cancer Hospital and Institute, Beijing 100000, China

[3]Department of surgical oncology, ChuiYangLiu Hospital affiliated to Tsinghua University, Beijing 100000, China

[4]Center for Reproductive Medicine, Peking University Third Hospital, Beijing 100000, China

[5]Key Laboratory of Assisted Reproduction, Ministry of Education, Beijing 100000, China

[6]College of Animal Science and Veterinary Medicine, Heilongjiang Bayi Agricultural University, Daqing 163000, China

[7]Institute of Immunology, Tsinghua University School of Medicine, Beijing 100000, China

[8]These authors contributed equally

[9]Lead contact

*Correspondence: drwuaw@sina.com (A.W.), limo@hsc.pku.edu.cn (M.L.), fupingyou@hsc.pku.edu.cn (F.Y.)

https://doi.org/10.1016/j.isci.2021.102169

reprogram normal cells for genome alteration accumulation. However, evidence supporting this model is largely lacking, and whether epigenetic priming includes suppression of DNA repair response has not been explored.

Here, we showed that suppression of ELF4 predisposes host with UC to CAC. We identified ELF4 as an important element keeping intestinal epithelial genome safe, which upon PARylation by PARP1 transcriptionally regulates multiple DNA damage response (DDR) machinery components in active UC. ELF4 deficiency leads to more severe DNA damages both *in vitro* and *in vivo* causing host cells prone to tumorigenesis, while ELF4 is epigenetically suppressed in both patients with CAC and mouse models. We further showed that oral administration of montmorillonite powder, a commonly used intestinal mucosal protective agent, can prevent the reduction of ELF4 in DSS-induced colitis models. Moreover, our retrospective study demonstrated that patients with CAC regularly on montmorillonite treatment in early UC phase showed significantly delayed CAC development. These findings identify ELF4 as a key target of epigenetic priming during colon cancer evolution. Furthermore, our data suggest that montmorillonite powder might serve as an ideal CAC prevention drug for patients with UC.

RESULTS

ELF4 deficiency leads to hyper-susceptibility to CAC

The tissue expression pattern of ELF4 showed the highest expression in the colon of mice (Figures S1A–S1C) and high expression in colon epithelia in humans (Figure S1D) (Uhlen et al., 2005). To examine the role of ELF4 in UC pathogenesis, we induced chronic colitis in wild-type (WT) and *Elf4*$^{-/-}$ mice with 3 cycles of 1.5% DSS treatment (Figure 1A). The body weight loss showed slight difference (Figure 1B). However, we surprisingly found all of *Elf4*$^{-/-}$ mice developed tumors in the colon, while WT mice only showed moderate dysplasia (Figures 1C–1E). It is noteworthy that induction of colon tumors by DSS alone usually requires sufficient duration (more than 5 cycles, about 100 days) (Gkouskou et al., 2016; Okayasu et al., 2002). The susceptibility of *Elf4*$^{-/-}$ mice to colon tumor development was also significant using standard AOM/DSS protocol (Figures 1F–1J), although there was no difference in terms of histopathology for developed tumors compared to WT mice (Figures S1E and S1F). These data indicate that ELF4 plays a pivotal role in the initiation of CAC.

ELF4 suppression is prevalent in patients with UC and DSS-induced mice models

To determine the clinical relevance of ELF4, we collected endoscopic biopsy samples from patients with UC and healthy controls. Interestingly, we detected significant suppression of ELF4 at mRNA level (Figure 2A). To consolidate this finding, we mined the Gene Expression Omnibus database with web-based tool GEO2R (Table S1). We noticed that ELF4 was significantly decreased in the colon mucosa of patients with UC and active inflammation from two independent cohorts (Figures S2A and S2B). This deficiency of ELF4 was also found in non-dysplastic mucosa from patients with UC harboring remote neoplastic lesions (Figure S2C). In addition, we induced acute colitis with DSS in WT mice to mimic UC flare in patients and found similar suppression of ELF4 in mice colon mucosa with active inflammation (Figure 2B). A data set in the Gene Expression Omnibus (GEO) also supported this finding (Figure S2D). More interestingly, the distal colon with dysplasia and intramucosal adenocarcinoma also showed reduction of ELF4 in an AOM/DSS-induced CAC model (Figure S2E), which was further confirmed in our AOM/DSS CAC model (Figures 2C and 2D). Lastly, we found reduction of ELF4 in the cancer tissue of three patients with CAC (Figure 2E). These data suggested that ELF4 is an intriguing factor in inflammation-driven tumorigenesis and of great clinical relevance.

Intestinal epithelial ELF4 restrains colitis by supporting the function of ILC3s

The frequency and severity of UC flares is closely associated with CAC risk (Ekbom et al., 1990); we then reasoned that CAC predisposition might root in repeated colitis flare. Indeed, *Elf4*$^{-/-}$ mice showed poor survival (Figure 3A) and more severe body weight loss (Figure 3B) after being treated with an acute dose of DSS. Histologically, *Elf4*$^{-/-}$ mice showed more leukocytes infiltration, crypt elongation, and loss of goblet cells (Figures 3C and 3D). We previously found that ELF4 is essential for antiviral innate immunity (You et al., 2013). We thus investigated if deficiency of ELF4 in myeloid cells caused colon inflammation. We generated ELF4 conditional deficient mice by crossing *Elf4*$^{fl/fl}$ mice with Lyz2-Cre mice. Interestingly, *Elf4*$^{fl/fl}$-Lyz2-Cre mice showed comparable weight loss and lethality to WT mice after DSS treatment (Figures 3E and 3F). Therefore, *Elf4*$^{fl/fl}$-Villin-Cre mice were included to explore whether loss of colon epithelial ELF4 is responsible for increased inflammation (Figure S3A). We found that *Elf4*$^{fl/fl}$-Villin-Cre mice showed

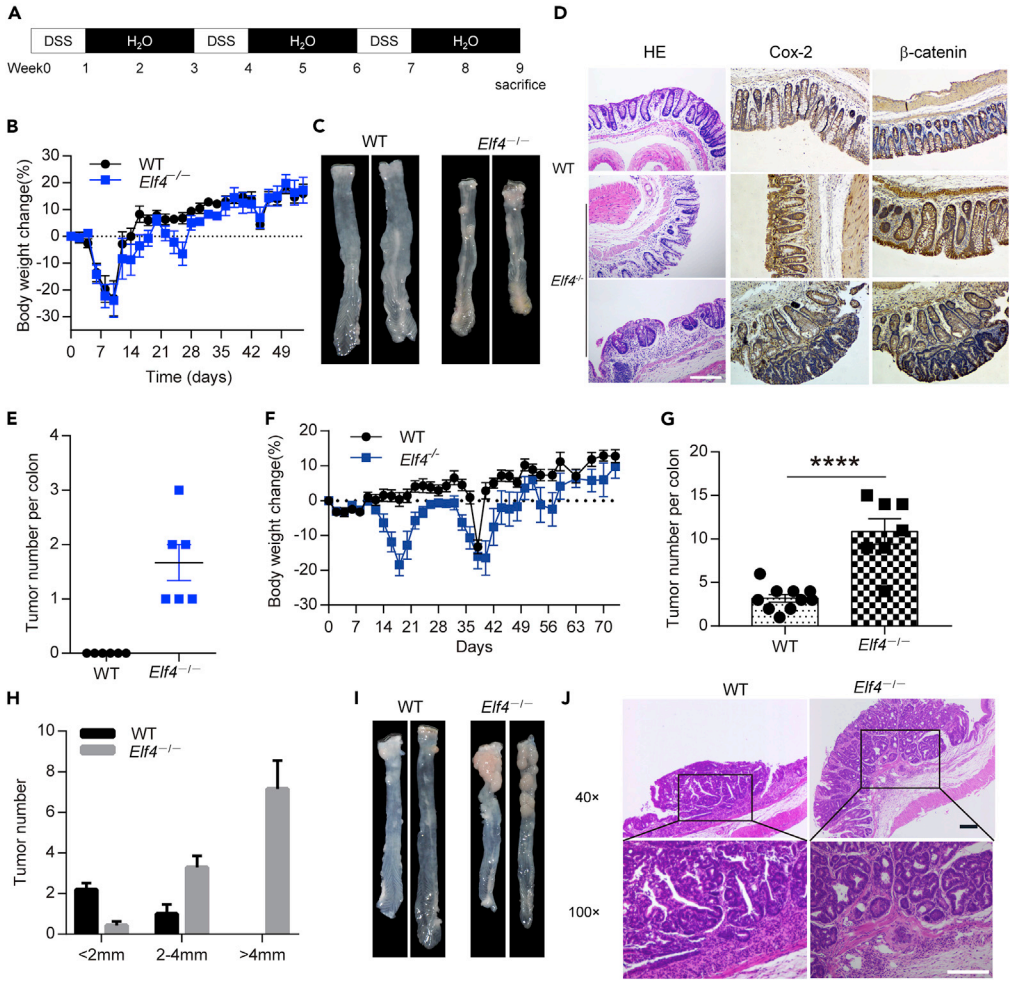

Figure 1. Elf4-deficient mice are hyper-susceptible to inflammation-driven colorectal cancer

(A) Schematic of DSS administration.

(B) Body weight change of indicated mice treated with low dose DSS (1.5%) protocol. WT, n = 6; *Elf4*$^{-/-}$, n = 6, data are represented as mean ± standard error of mean (SEM).

(C) Representative pictures of colon tumors.

(D) Representative H&E-stained, immunohistochemical Cox-2 and β-catenin-stained images of colon sections, scale bar: 200 um.

(E) Number of tumors in the whole colon was counted. WT, n = 6; *Elf4*$^{-/-}$, n = 6, data are represented as mean ± standard error of mean (SEM).

(F) Body weight change of indicated mice treated with standard AOM-DSS (1.5%) protocol. WT, n = 10; *Elf4*$^{-/-}$, n = 9, data are represented as mean ± standard error of mean (SEM).

(G) Number of tumors in the whole colon was counted. WT, n = 10; *Elf4*$^{-/-}$, n = 7. ****P = 3.64 × 10^{-5}. Unpaired two-sided Student' s *t* test, data are represented as mean ± standard error of mean (SEM).

(H) Representative distribution of the average number of tumors per mouse. WT, n = 10; *Elf4*$^{-/-}$, n = 7, data are represented as mean ± standard error of mean (SEM).

(I) Representative pictures of colon tumors.

(J) Representative H&E-stained images of colon sections, scale bar: 200 um.

See also Figure S1.

similar phenotypes with *Elf4*$^{-/-}$ mice after DSS treatment (Figures 3G and 3H). It suggested that intestinal epithelium ELF4 but not myeloid cell ELF4 restrains colitis.

The inflamed colons of WT and *Elf4*$^{-/-}$ mice were subjected to whole genome RNA sequencing. We found that Elf4 deficiency led to a significantly different transcriptional response to DSS treatment, as

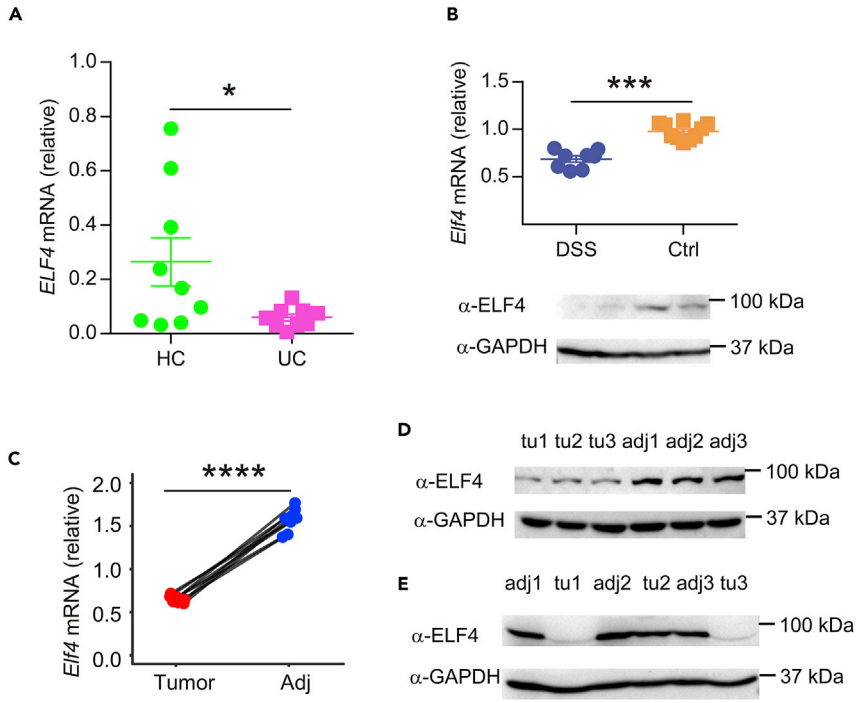

Figure 2. ELF4 deficiency is prevalent in patients with UC and CAC and mice models

(A) Comparison of *ELF4* mRNA level in colon mucosa between 9 healthy donors and 9 patients with active UC. *P = 0.0359. Unpaired two-sided Student' s *t* test, data are represented as mean ± Standard Error of Mean (SEM).

(B) Comparison of *Elf4* mRNA and protein level in colon mucosa between regular water drinking and DSS drinking wild-type mice. D, DSS drinking, n = 10; W, water drinking, n = 8. ****P = 4.02×10^{-6}. Unpaired two-sided Student' s *t* test, data are represented as mean ± Standard Error of Mean (SEM).

(C) Comparison of *Elf4* mRNA level between tumor adjacent and tumor tissue in wild-type mice treated with standard AOM/DSS protocol. n = 8. Tumor, tumor tissue; Adj, tumor adjacent tissue. ****P = 2.79×10^{-7}, paired Student's *t*-test.

(D) Comparison of Elf4 protein level between tumor adjacent and tumor tissue in wild-type mice treated with standard AOM/DSS protocol. Tu1, tu2, and tu3 were tumor tissues; adj1, adj2, and adj3 were tumor adjacent tissues.

(E) Comparison of ELF4 protein level between adjacent and cancer tissue in 3 patients with CAC. Tu1, tu2, and tu3 were tumor tissues; adj1, adj2, and adj3 were tumor adjacent tissues.

See also Figure S2 and Table S1.

demonstrated by general transcriptome dissimilarity (Figure S3B). Among 16,788 detected genes, there are a total of 1980 genes upregulated in *Elf4*$^{-/-}$ mice and 2141 genes downregulated in *Elf4*$^{-/-}$ mice (Figure S3C). We also did whole-genome RNA sequencing of inflamed colons of WT and *Elf4*$^{fl/fl}$-Villin-Cre mice treated with 2% DSS for 5 days. Gene set enrichment analysis showed pathways enriched in *Elf4*$^{fl/fl}$-Villin-Cre mice mainly focus on inflammatory response, the activation and regulation of macrophages, the migration of monocytes, and cell chemotaxis (Figure S3D). Differentially expressed gene analysis showed that expression of certain mucin genes and regenerating gene (REG) was significantly lower in *Elf4*$^{-/-}$ mice. We then confirmed the difference using quantitative reverse transcription-PCR (RT-qPCR) (Figures S3E and 3I). Mucin and REG proteins play important roles in the pathogenesis of UC and CAC. For example, *Muc2*-deficient mice spontaneously develop colitis and adenomas, which develop into invasive adenocarcinomas (Heazlewood et al., 2008; Velcich et al., 2002). *Reg3γ*-deficient mice also spontaneously develop colitis (Loonen et al., 2014). Reg3β and Reg3γ are critical for intestinal microbiota homeostasis and tissue repair (Wells et al., 2017). Severely impaired mucin and REG protein expression led to the breakdown of colonic epithelial barrier, which exacerbated inflammation.

In the intestine, ILC3s play an important role in regulating tissue repair through their major effector IL-22 (Mielke et al., 2013; Sonnenberg and Artis, 2015). IL-22 signaling induces the generation of mucin and REG proteins to facilitate tissue repair. To further explore the barrier protection role of ELF4, we investigated the function of ILC3s in *Elf4*$^{-/-}$ mice. We found intestinal ILC3s were normally developed in *Elf4*$^{-/-}$

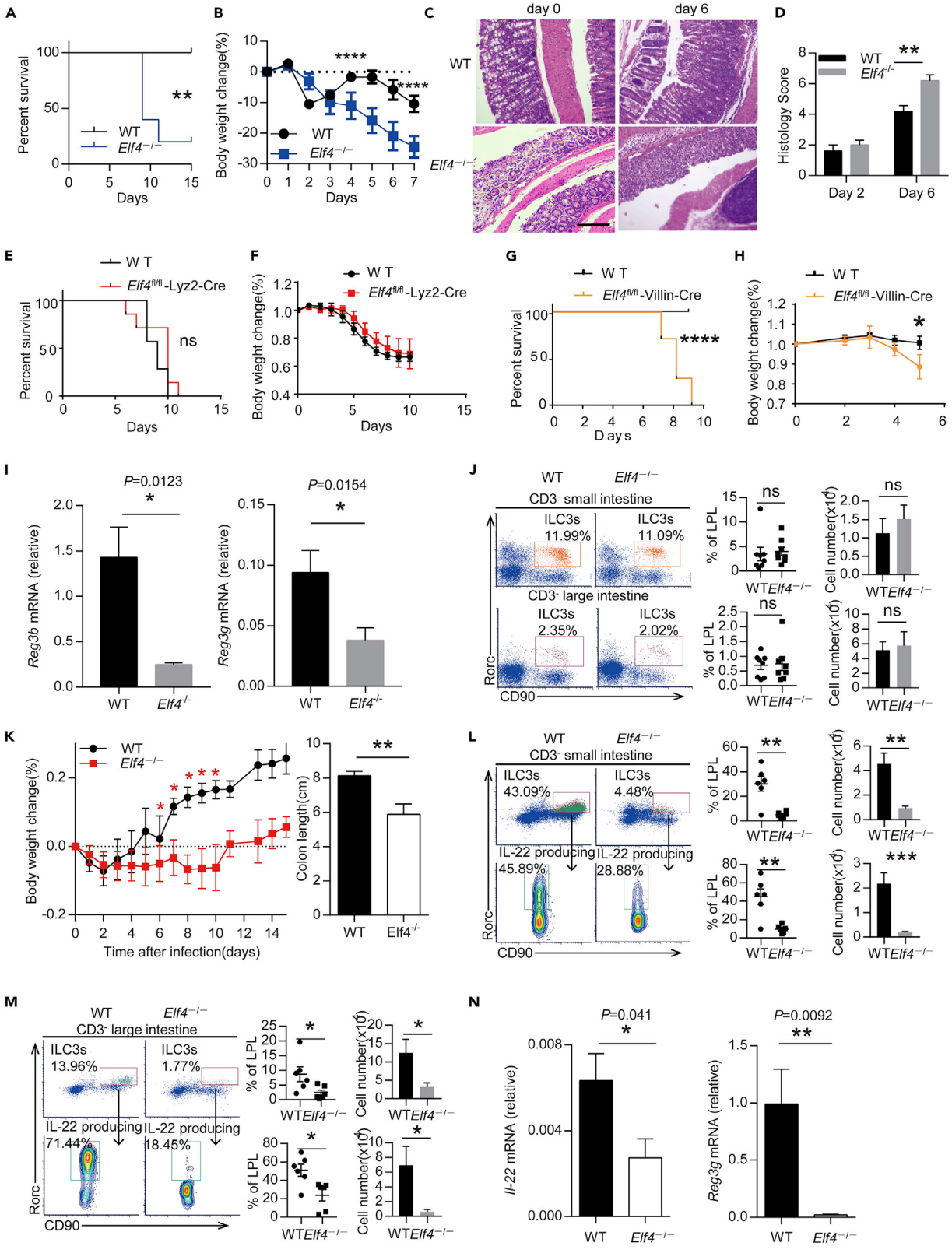
A
Percent survival
Days
WT
Elf4−/−
**
B
Body weight change(%)
Days
****
C
day 0
day 6
WT
Elf4−/−
D
Histology Score
Day 2
Day 6
**
E
Elf4fl/fl-Lyz2-Cre
ns
F
Body wieght change(%)
G
Elf4fl/fl-Villin-Cre
****
H
Body weight change(%)
*
I
P=0.0123
Reg3b mRNA (relative)
P=0.0154
Reg3g mRNA (relative)
J
CD3- small intestine
CD3- large intestine
ILC3s
11.99%
11.09%
2.35%
2.02%
Rorc
CD90
% of LPL
Cell number(x10⁴)
ns
K
Body weight change(%)
Time after infection(days)
Colon length(cm)
L
ILC3s
43.09%
4.48%
IL-22 producing
45.89%
28.88%
***
M
ILC3s
13.96%
1.77%
IL-22 producing
71.44%
18.45%
N
P=0.041
Il-22 mRNA (relative)
P=0.0092
Reg3g mRNA (relative)

Figure 3. Intestinal epithelium Elf4 is critical for multiple colon mucosa protecting factors

(A) Mortality of age- and sex-matched wild-type and *Elf4*$^{-/-}$ mice treated with standard DSS-induced acute colitis protocol. WT, n = 6; *Elf4*$^{-/-}$, n = 5. **P = 0.0070, log-rank (Mantel-Cox) test.

(B) Body weight change of indicated mice. WT, n = 10; *Elf4*$^{-/-}$, n = 10. Day 4, ****P < 0.0001. Unpaired two-sided Student' s *t* test, data are represented as mean ± standard error of mean (SEM).

(C) Representative H&E-stained images of colon sections, scale bar: 200 um.

(D) Histology score of inflammation at indicated time. WT, n = 10; *Elf4*$^{-/-}$, n = 10. **P = 0.005. Unpaired two-sided Student' s *t* test, data are represented as mean ± standard error of mean (SEM).

(E and F) Mortality (E) and body weight percent (F) of six-week-old male wild-type and *Elf4*$^{fl/fl}$-Lyz2-Cre mice treated with 2% DSS for 7 days. WT, n = 7, *Elf4*$^{fl/fl}$-Lyz2-Cre, n = 7. NS, not significant. Data are represented as mean ± standard error of mean (SEM).

(G) Mortality of six-week-old male wild-type and *Elf4*$^{fl/fl}$-Villin-Cre mice treated with 1.5% DSS for 5 days. WT, n = 4, *Elf4*$^{fl/fl}$-Villin-Cre, n = 7. ****P < 0.0001, log-rank (Mantel-Cox) test.

(H) Body weight percent of six-week-old female wild-type and *Elf4*$^{fl/fl}$-Villin-Cre mice treated with 2% DSS for 5 days. WT, n = 4, *Elf4*$^{fl/fl}$-Villin-Cre, n = 3. *P = 0.0186. Unpaired two-sided Student' s *t* test, data are represented as mean ± standard error of mean (SEM).

(I) Comparison of indicated genes between DSS-treated WT and *Elf4*$^{-/-}$ mice by RT-qPCR. WT, n = 5; *Elf4*$^{-/-}$, n = 5. *P < 0.05. Unpaired two-sided Student' s *t* test, data are represented as mean ± standard error of mean (SEM).

(J) Left, flow cytometry analyzing ILC3s (CD3^{-}CD90^{+}RORγt^{+}) from the small intestine (upper) and large intestine (lower); right, frequency and the total number of ILC3s in lamina propria lymphocytes from the small intestine (upper) and large intestine (lower) (n = 8 per genotype). Data are represented as mean ± standard error of mean (SEM).

(K) Body weight change (left) and colon length (right) of indicated mice after being infected with *C. rodentium* (n = 6 per genotype). Day 7, day 8, day 9, day 10, *P < 0.05, **P = 0.005. Unpaired two-sided Student' s *t* test, data are represented as mean ± standard error of mean (SEM).

(L) Left, flow cytometry analyzing IL-22-producing ILC3s (CD3^{-}CD90^{+}RORγt^{+}IL-22^{+}) from the small intestine; right, frequency and the total number of IL-22-producing ILC3s in lamina propria total ILC3s from the small intestine (n = 6 per genotype). Unpaired two-sided Student' s *t* test, data are represented as mean ± standard error of mean (SEM).

(M) Left, flow cytometry analyzing IL-22-producing ILC3s (CD3^{-}CD90^{+}RORγt^{+}IL-22^{+}) from the large intestine; right, frequency and the total number of IL-22-producing ILC3s in lamina propria total ILC3s from the large intestine (n = 6 per genotype). Unpaired two-sided Student' s *t* test, data are represented as mean ± standard error of mean (SEM).

(N) Comparison of indicated genes between *C. rodentium* infected WT and *Elf4*$^{-/-}$ mice by RT-qPCR (n = 6 per genotype). *P = 0.0407; **P = 0.0092. Unpaired two-sided Student' s *t* test, data are represented as mean ± standard error of mean (SEM).

See also Figure S3.

mice at the resting state (Figure 3J). We then challenged WT and *Elf4*$^{-/-}$ mice with *C. rodentium* to test the function of ILC3s. *Elf4*$^{-/-}$ mice were more susceptible to *C. rodentium* infection and showed more severe inflammation (Figure 3K). ILC3s from *Elf4*$^{-/-}$ mice showed smaller number and dampened capability to produce IL-22 in response to IL-23 stimulation compared to WT mice (Figures 3L and 3M). RT-qPCR results supported this finding (Figure 3N). Thus, impaired ILC3 function also contributed to the vulnerability of intestinal barrier of *Elf4*$^{-/-}$ mice. Collectively, these data suggested that the intestinal epithelial ELF4 was critical for mucin protein expression and ILC3 function.

ELF4 promotes DNA damage repair by upregulating DDR machinery components

As mentioned above, genomic mutation accumulation is a key step of tumorigenesis. It has been reported that ELF4 can promote the faster repair of damaged DNA in response to γ-irradiation (Sashida et al., 2011), so we focus on whether ELF4 suppression in the development of CAC will lead more DNA damage. Expression of a set of DNA damage response pathway genes was significantly lower in *Elf4*$^{-/-}$ mice compared to control mice (Figure 4A). These genes play essential roles in various DNA damage responses (DDR) (Table S2). To confirm this finding, we replicated the experiment with a larger sample number. Indeed, *H2ax*, *Taok3*, *Nabp1*, *Nbn*, *Fbxo18*, and *Ints3* were all decreased in *Elf4*$^{-/-}$ mice (Figure 4B) and ELF4 knockdown cell lines (Figure S4A). The protein level of H2AX showed consistent decrease (Figures 4C and S4B).

Based on this observation and the hyper-susceptibility of *Elf4*$^{-/-}$ mice to CAC, we hypothesized that ELF4 might play an important role in keeping colon epithelial genome safe by regulating a spectrum of key components of DDR machinery. To further confirm this, the *Elf4*$^{-/-}$ cells were established in NCM460 and SW480, the former a normal human colon mucosal epithelial cell line (Moyer et al., 1996) and the latter derived from human colon cancer. Comet assays showed that there was more DNA damage in *Elf4*$^{-/-}$ SW480 cells (Figures 4D and S4C) and *Elf4*$^{-/-}$ NCM460 cells (Figures S4D and S4E) in response to H_2O_2 treatment compared to control groups. 8-oxo-dG (8-Oxo-7,8-dihydro-2′-deoxyguanosine) is an excellent marker for DNA damage produced by oxidants because it represents one of the major products generated by a wide array of treatments associated with oxidant damage (Roszkowski et al., 2011). We detected much

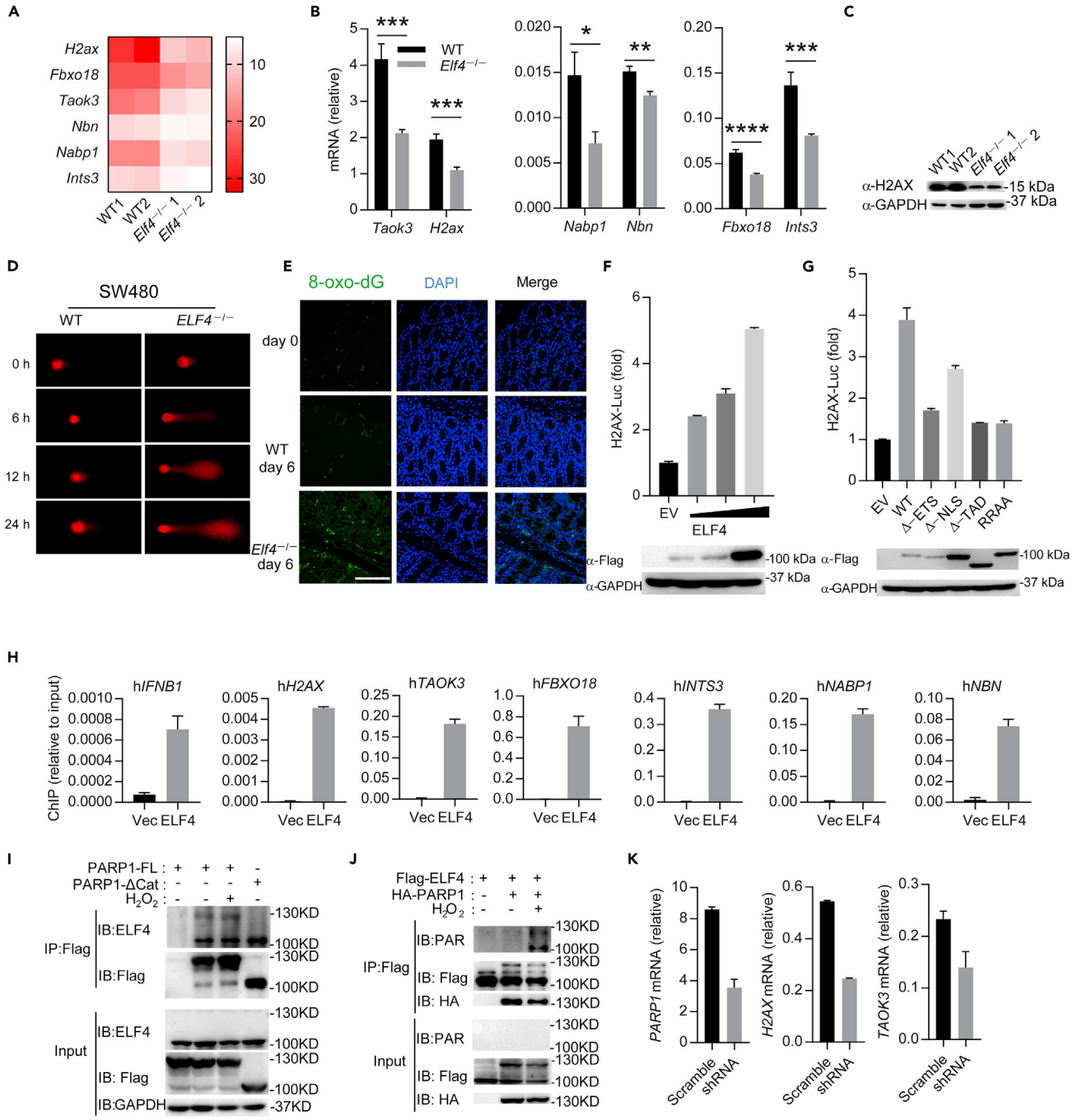

Figure 4. Elf4 is a master transcription regulator of DNA damage response.

(A) Heatmap representing selected DNA damage response genes of indicated mice.

(B) Comparison of indicated genes between DSS-treated WT and *Elf4*$^{-/-}$ mice by RT-qPCR. WT, n = 5; *Elf4*$^{-/-}$, n = 5. *P = 0.016, **P = 0.0024, ***P < 0.001, ****P = 1.07 × 10^{-5}. Unpaired two-sided Student' s *t* test, data are represented as mean ± standard error of mean (SEM).

(C) Comparison of H2AX in colon mucosa between wild-type and *Elf4*$^{-/-}$ mice treated with DSS at day 6.

(D) Representative images of Comet assay in WT and *ELF4*$^{-/-}$ SW480 cells treated with H_2O_2 for indicated time.

(E) Representative immunostaining for DAPI (blue) and 8-oxo-dG (green) and co-staining (merge) in the colon of indicated mice, scale bar: 200 um.

(F and G) Luciferase assay of HEK 293T cells transfected with H2AX-luc plasmid and indicated expression plasmids. Data were pooled from three independent experiments; data are represented as mean ± standard error of mean (SEM).

(H) ChIP-qRT-PCR experiments showing Flag-ELF4 binding to indicated promoters in SW480 cells stably expressing ELF4 and control vector. h*IFNB1* promoter serves as positive control; data are represented as mean ± standard error of mean (SEM).

Figure 4. *Continued*

(I) Immunoprecipitation of Flag-tagged full-length PARP1 and catalytic domain deleted PARP1. First lane is IgG control.

(J) Flag-tagged ELF4 was co-immunoprecipitated with HA-tagged PARP1.

(K) mRNA levels of *H2AX* and *TAOK3* when *PARP1* was knocked down with shRNA; data are represented as mean ± Standard Error of Mean (SEM).

See also Figure S4, Tables S2 and S3.

more 8-oxo-dG in the colon epithelia of *Elf4*$^{-/-}$ mice treated with 1 cycle of DSS (Figures 4E and S4F), indicating impaired DDR in *Elf4*$^{-/-}$ mice.

Next, to test the possibility that ELF4 transcriptionally regulated these genes, we constructed promoter luciferase reporters of *H2AX*, *NABP1*, *FBXO18*, and *TAOK3*. Overexpression of ELF4 in HEK 293T showed that ELF4 activated these promoters in a dose-dependent manner (Figures 4F and S4G). To identify the critical domains of ELF4 required for these processes, we constructed a series of deletion and mutation mutants of ELF4. We found that the ETS domain, nuclear localization sequence region, and transactivation domain (amino acids 1–87) were all indispensable for induction of H2AX, FBXO18, TAOK3, and NABP1 expression (Figures 4G and S4G), similar to the case of IFNB1 induction (You et al., 2013). Two highly conserved arginines in the ETS domain are critical for DNA binding (Wei et al., 2010). Replacing these two arginines with alanines (ELF4-RRAA) also abrogated activation of *H2AX*, *FBXO18*, *TAOK3*, and *NABP1* promoters (Figures 4G and S4G). Mining Elf4 ChIP-seq data with Cistrome Data Browser showed endogenous evidence that Elf4 indeed binded to the promoters of *H2ax*, *Taok3*, *Fbxo18*, *Nabp1*, *Nbn*, and *Ints3* (Figure S4H) (Curina et al., 2017; Mei et al., 2017). We confirmed these bindings in SW480 cells stably expressing ELF4 by Chromatin immunoprecipitation (ChIP) coupled to quantitative PCR (ChIP-qPCR) assay (Figure 4H).

In an effort to identify ELF4-interacting partners, we found PARP1 is a potential candidate in a Flag-tagged ELF4 overexpression system by mass spectrometry (Table S3). PARP1 is a well-known DNA damage sensor (Ray Chaudhuri and Nussenzweig, 2017). We thus reasoned that PARP1/ELF4 DNA damage response axis might be the biological relevance of this interaction. We confirmed this interaction by co-immunoprecipitation (Figure 4I). Interestingly, we noticed a band shift of ELF4 by PARP1 overexpression, which was dependent on the catalytic domain of PARP1 (Figure 4I). We repeated this experiment in a dual overexpression system. The band of ELF4 was similarly shifted (Figure 4J). In addition, when we incubated the replicative lanes with anti-PAR antibody, we found bands of same size with main ELF4 and shifted ELF4, indicating ELF4 was PARylated by PARP1 (Figure 4J). Furthermore, knockdown of PARP1 led to similar reduction of H2AX and TAOK3 (Figure 4K). Thus, upon PARylation by PARP1, ELF4 might play an important role in keeping colon epithelial genome safe, and ELF4 deficiency predisposed host to mutagenesis and tumorigenesis.

Collectively, on the one hand, ELF4 was critical for mucin protein expression, which anatomically shielded colon epithelia and probably the colon stem cells from the actions of carcinogens (Bischoff et al., 2014). On the other hand, ELF4 supported the transcription of multiple DDR machinery components to ensure a competent DDR.

Suppression of ELF4 in CAC depends on its promoter methylation

We next asked how ELF4 was suppressed in CAC. It is well recognized that tumorigenesis is a multi-step process marked by a series of genetic and epigenetic alterations (Hanahan and Weinberg, 2011). In this model, the driver mutation signals the beginning of the long evolution and selection process toward malignancy. Recently, the phenomenon of "trained immunity" indicates that cells can be transformed by epigenetic reprogramming (Netea et al., 2016). So, we hypothesized that before the genetic reprogramming stage, there was an epigenetic reprogramming stage, which created a mutation-prone environment. ELF4 suppression could be such an example. The *ELF4* promoter region showed CpG island enrichment in human colon cells; we predicted and got two CpG regions (region A and region B) by MethPrimer (Figure S5A) (Akhtar-Zaidi et al., 2012; Li and Dahiya, 2002; Mei et al., 2017). In order to make sure which region is mainly responsible to transcriptional regulation of ELF4, we constructed luciferase reporters of *ELF4* promoter region A, *ELF4* promoter region B, and *ELF4* promoter full length. Overexpression of ELF4 in SW480 (Figure 5A) and NCM460 (Figure S5B) showed region A is mainly responsible for ELF4 transcriptional regulation. In CAC tissue, *ELF4* promoter region A methylation should be responsible for the more stable suppression (Figure 5B), and we also observed that the *Elf4* promoter methylation level of tumor tissue induced by AOM-DSS protocol is higher than that of peripheral tissue (Figure 5C). IL-6 can induce promoter hypermethylation of tumor suppressor genes via DNMT1 (Li et al., 2012). We showed that IL-6 treatment suppressed ELF4 in NCM460 and SW480 cells (Figure 5D), and this suppression was also dependent

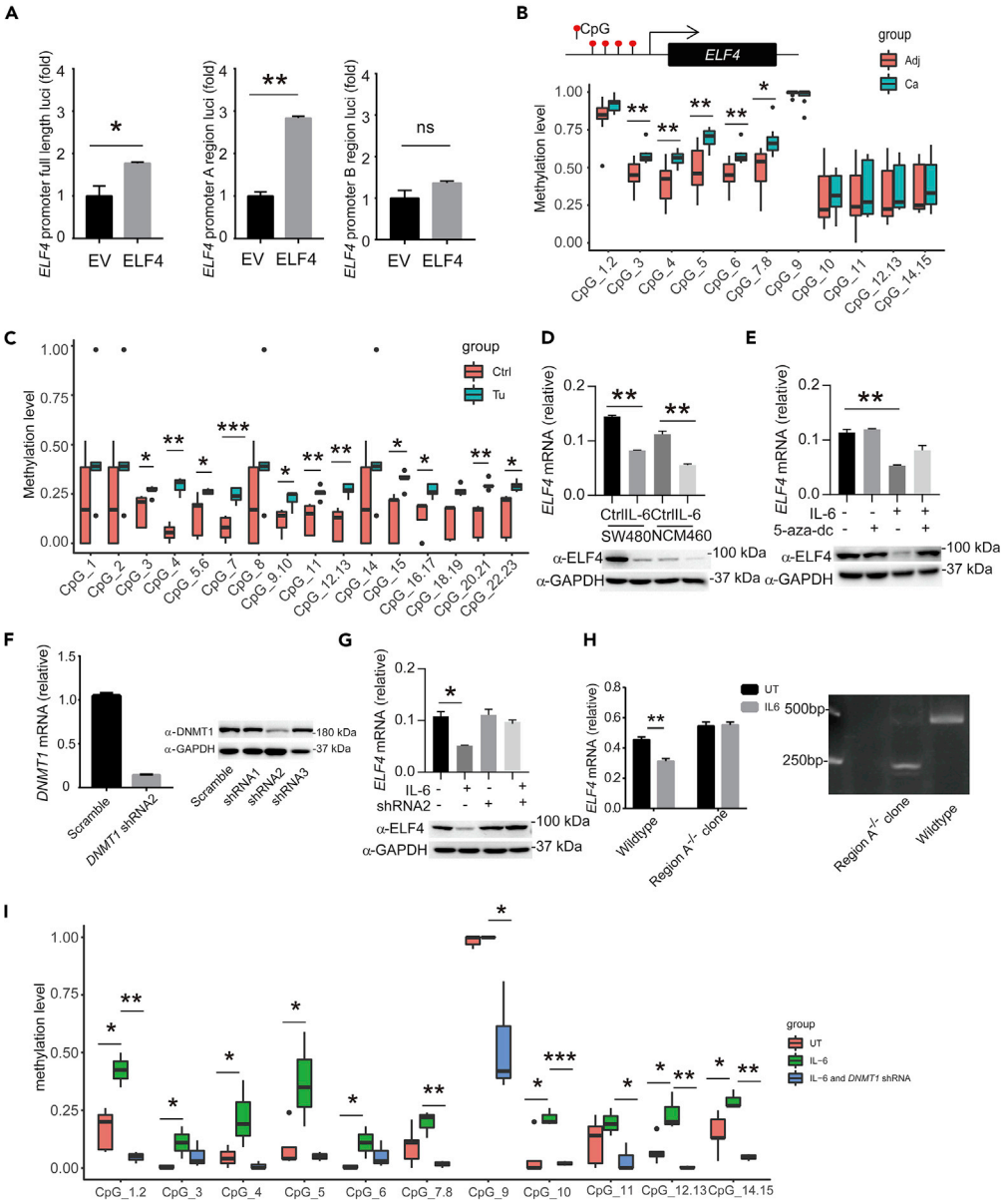

Figure 5. ELF4 is epigenetically suppressed in CAC

(A) Luciferase assay of SW480 cells transfected with ELF4 promoter full length or truncation luciferase plasmid and indicated expression plasmids. *P = 0.0443, **P = 0.0016, ns, not significant. Unpaired two-sided Student' s *t* test, data are represented as mean ± standard error of mean (SEM) Data were pooled from three independent experiments.

(B) Quantitative methylation analysis on each CpG site in a selected *ELF4* promoter region in paired clinical samples from 8 patients with CAC. Methylation level 1 represents 100% methylated CpG dinucleotides on this site. Adj, cancer adjacent tissue; Ca, cancer tissue. *P = 0.0141, **P < 0.01. Unpaired two-sided Student' s *t* test, data are represented as mean ± standard error of mean (SEM).

(C) Quantitative methylation analysis on each CpG site in a selected *Elf4* promoter region in paired mice CAC samples. *P < 0.05, **P < 0.01, ***P = 0.0009. Unpaired two-sided Student' s *t* test, data are represented as mean ± standard error of mean (SEM).

(D) *ELF4* mRNA (top) and protein (bottom) level change after IL-6 treatment in SW480 and NCM460 cells. **P < 0.01. Unpaired two-sided Student' s *t* test, data are represented as mean ± standard error of mean (SEM).

(E) Analysis of DNMT1 inhibitor 5-aza-dc on IL-6 induced suppression of ELF4 in SW480 cells. **P = 0.0082. Unpaired two-sided Student' s *t* test, data are represented as mean ± standard error of mean (SEM).

(F) Knockdown efficiency of *DNMT1* shRNA measured by qPCR (left) and immunoblot (right), data are represented as mean ± standard error of mean (SEM).

Figure 5. *Continued*

(G) Effects of DNMT1 knockdown on IL-6 induced suppression of ELF4 in SW480 cells. *P = 0.0222. Unpaired two-sided Student' s *t* test, data are represented as mean ± standard error of mean (SEM).

(H) Effects of region CpG1-11 deletion of *ELF4* promoter on IL-6 induced *ELF4* suppression in SW480 cells (left). Nucleic acid gel electrophoresis to identify the deletion of region CpG1-11 of *ELF4* promoter (right). **P = 0.0043. Unpaired two-sided Student' s *t* test, data are represented as mean ± standard error of mean (SEM).

(I) Quantitative methylation analysis on each CpG site in a selected *ELF4* promoter region (region A) in untreated, IL-6 treated, or IL-6 and DNMT1 shRNA2-treated SW480 cells. *P < 0.05, **P < 0.01, ***P < 0.001. Unpaired two-sided Student' s *t* test, data are represented as mean ± standard error of mean (SEM).

See also Figure S5.

on DNMT1 (Figures 5E–5G). To further investigate the mechanism of ELF4 suppression, we used clustered regularly interspaced short palindromic repeats (CRISPR)/CRISPR-associated (Cas) protein 9 system to delete the region A of *ELF4* promoter in SW480 cells (Figure S5C). As shown in Figure 5H, IL-6 treatment can only suppress ELF4 expression in WT SW480 cells, while the ELF4 suppression effect and ELF4 promoter methylation level increase of IL-6 treatment is abolished by DNMT1 shRNA treatment (Figures 5G and 5I). Thus, before any genetic changes, there is an epigenetic reprogramming stage preparing the cell for transformation by creating a mutation-prone transcriptional environment.

Oral administration of montmorillonite rescues ELF4 expression and lowers risk of CAC development

We next asked what can rescue Elf4 expression. Tissue damage and epithelium disruption is a major histopathologic feature in UC, which exposes mucosal immune cells directly to various stimuli, causing diverse cellular responses (Martini et al., 2017). Montmorillonite, a natural dioctahedron phyllosilicate, is a commonly used intestinal mucosal protective agent for diarrhea (Dupont and Vernisse, 2009; Gonzalez et al., 2004), which increases the resistance of the intestinal epithelium to toxic stimuli in humans (Dupont et al., 2009). We then hypothesized that montmorillonite could also protect the intestinal barrier during active colitis and prevent ELF4 suppression by reducing inflammation. We found that oral administration of montmorillonite powder prevented Elf4 suppression (Figure 6A) and significantly attenuated DNA damage in colon mucosa (Figures 6B and S6A). Histologically, intestinal structure of the montmorillonite powder treatment group is more complete compared with the control group (Figure S6B). The mRNA expression of *Elf4* and *Dnmt1* was negatively correlated (Figures S6C–S6E) after treatment with montmorillonite powder, and we did observe a decrease in the Elf4 promoter methylation level difference after montmorillonite powder treatment, although not statistically significant (Figure S6F).

To further test the cancer prevention potential of montmorillonite, we added montmorillonite powder treatment during CAC induction course by AOM/DSS in mice. As expected, $Elf4^{fl/fl}$ CAC mice treated with montmorillonite powder showed less colon tumor development, while $Elf4^{fl/fl}$-Villin-Cre mice showed no response (Figure 6C). The hematoxylin and eosin (H&E) staining shows that tumors of $Elf4^{fl/fl}$-Villin-Cre mice represent features of adenocarcinomas (Figure S7A). Moreover, we did a retrospective study of 18 patients with CAC from Peking University Cancer Hospital between 2013 and 2018 (Table S4), who were grouped as never taken montmorillonite powder (n = 12), occasionally taken montmorillonite powder (n = 3), and regularly taken Montmorillonite powder (n = 3). The result showed that 3 of them who were regularly on montmorillonite powder treatment in addition to use of anti-inflammation drug during UC activation showed delayed development of CAC (Figure 6D), although the tumor number and size grading showed no difference (Figure 6E). CA19-9, one of the cancer biomarker tested, was significantly lower in these three patients (Figure 6F). These data suggested that montmorillonite powder might be a good candidate drug for CAC prevention.

DISCUSSION

IBD now affects between one in 200 and one in 300 people in developed countries (Ng et al., 2018). The prevalence in developing countries is still much lower than this, but the incidence is increasing rapidly. In China, for example, these conditions have changed from being rare to common (Zhao et al., 2013). Based on the large population China and other developing countries have, CAC could also be much more common in the next few decades. Etiologically, extensive studies have highlighted the importance of inflammation in the development of CAC (Grivennikov, 2013). In this study, we demonstrate that suppression of ELF4-mediated DDR also contributes to the development of CAC.

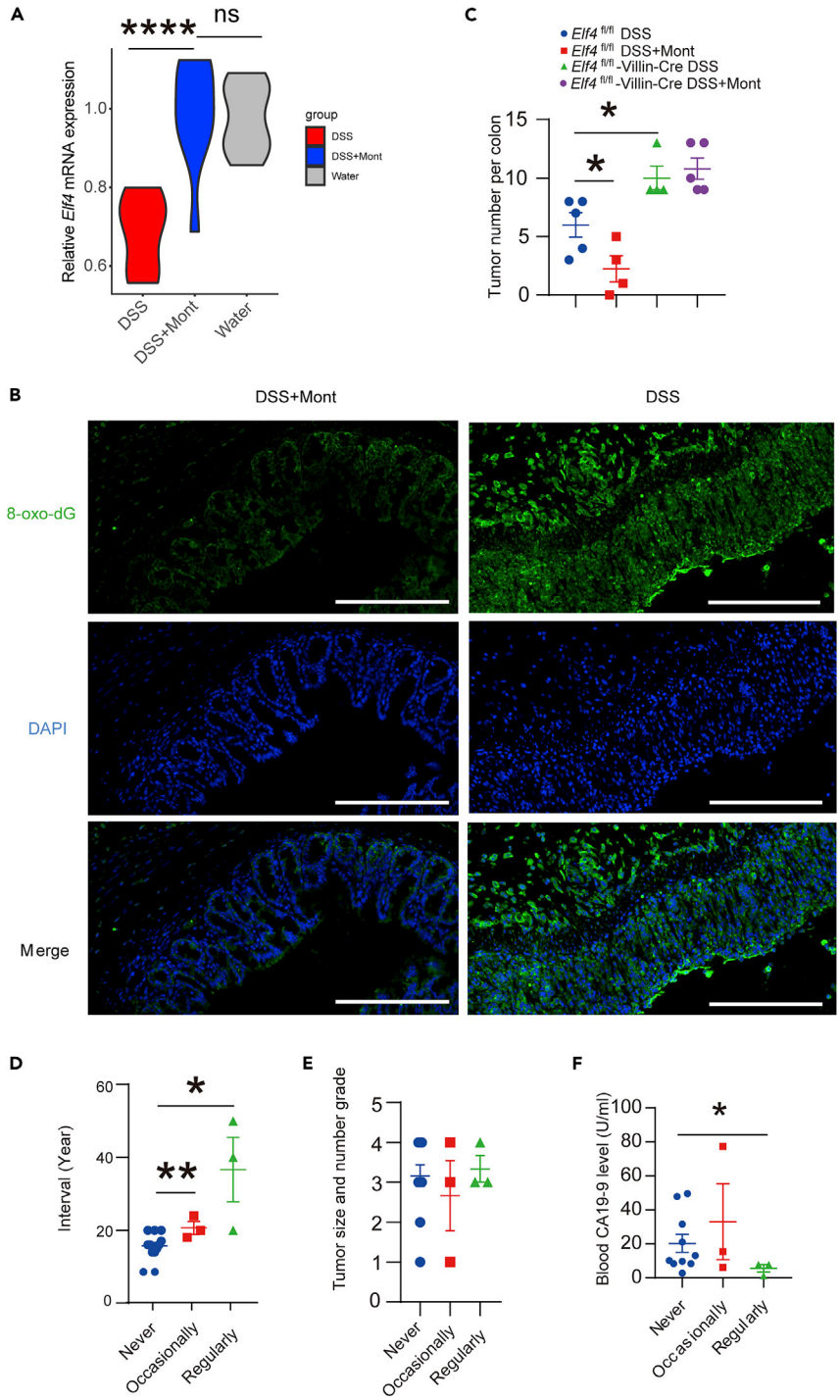

Figure 6. Montmorillonite restrains CAC through rescuing Elf4 expression

(A) Effects of montmorillonite powder on DSS induced suppression of *Elf4*, ****P = 4.02 × 10^{-6}, ns, not significant. Unpaired two-sided Student' s *t* test.

(B) Representative immunostaining for DAPI (blue) and 8-oxo-dG (green) and co-staining (merge) in the colon of indicated mice. Scale bar: 200 um.

(C) Tumor number count of indicated group of mice treated with standard AOM-DSS protocol. $Elf4^{fl/fl}$ DSS, n = 5, $Elf4^{fl/fl}$ DSS plus montmorillonite powder, n = 4, $Elf4^{fl/fl}$-Villin Cre DSS, n = 4, $Elf4^{fl/fl}$-Villin Cre DSS plus montmorillonite, n = 5. *P < 0.05. Unpaired two-sided Student' s *t* test, data are represented as mean ± standard error of mean (SEM).

Figure 6. *Continued*

(D) Eighteen patients with CAC were grouped as never taken montmorillonite powder (n = 12), occasionally taken montmorillonite powder (n = 3), and regularly taken Montmorillonite powder (n = 3). Comparisons of UC and CAC interval time duration among groups are shown. ***P = 0.0003, *P = 0.0386. Unpaired two-sided Student' s *t* test, data are represented as mean ± standard error of mean (SEM).

(E) Grading scores from the TNM staging system were compared. The T of TNM refers to the size and extent of the main tumor, data are represented as mean ± standard error of mean (SEM).

(F) Blood CA19-9 level before surgery. Mann-Whitney test, *P = 0.028. Unpaired two-sided Student' s *t* test, data are represented as mean ± standard error of mean (SEM).

See also Figures S6 and S7 and Table S4.

In sporadic CRC, tumors do not arise in the context of preceding inflammation, while in the case of CAC, clinically detectable IBD always precedes (sometimes by decades) tumor initiation. Inflammation indeed plays a significant role in CAC initiation and promotion (Terzic et al., 2010). In CAC, the hallmark of chronic inflammation is its ability to cause mutations. Colitis induces robust production of reactive oxygen species (ROS) and reactive nitrogen intermediates, which are highly reactive and mutagenic (Hussain et al., 2003; Meira et al., 2008). These oxidative DNA damages could lead to mutations of critical driver genes such as p53 in tumor cells and the inflamed but nondysplastic epithelium (Long et al., 2017). In mice, repeated DSS treatment can cause a low incidence of colonic adenomas (*17*), which is also thought as a result of inflammation-induced DNA damage (Meira et al., 2008). Our data showed that suppression of DDR is also an important contributor to colonic adenomas in colitis. Besides recruiting and activating nuclear complexes, PARP1 also exerts its effects by directly modifying protein activity and localization. Transcription factors such as Oct-1 and hnRNP K (heterogeneous nuclear ribonucleoprotein K) are known targets of PARP1, which, when ADP-ribosylated, are repelled from DNA, hence resulting in altered transcript expression profiles (Gagné et al., 2003; Nie et al., 1998). PARP1 sensed DNA damage and activated ELF4 through PARylation. ELF4 then bound to the promoters of multiple DNA repair genes, including *H2AX*, *FBXO18*, *TAOK3*, *NBN*, *NABP1*, and *INTS3*, and ensured potent transcription. ELF4 deficiency led to decreased expression of these genes and increased DNA damage *in vivo and in vitro*. H2AX upregulation and activation is an important signal to tell the cells that DNA damages occurred and initiated DNA repair process (Mah et al., 2010). With compromised downregulation of H2AX due to ELF4 downregulation, DNA damage repair machinery failed to repair genome efficiently, leading faster mutation accumulation, which predisposed cell to be cancerous. Nevertheless, we cannot rule out the possibility that ELF4 promotes DDR in additional transcription activity independent ways (Malewicz and Perlmann, 2014; Sashida et al., 2011), as a previous report showed that ELF4 translocated to DNA damage site in response to irradiation (Sashida et al., 2011).

Inflammation-induced mutagenesis can also cause inactivation or repression of mismatch repair genes, and ROS can directly oxidize and inactivate mismatch repair enzymes at protein level (Colotta et al., 2009; Hussain et al., 2003). However, ELF4 suppression is not genetic but epigenetic. Inflammation can also drive various epigenetic changes to silence genes during IBD and CAC. For example, DNA promoter methylation of tumor suppressor genes, such as *RUNX3*, *MINT1*, and *SOCS3*, has been reported in CAC (Emmett et al., 2017; Li et al., 2012). DNA methyltransferases Dnmt1 were shown to be upregulated and activated by inflammatory cytokines such as IL-6 highly produced in UC and CAC (Foran et al., 2010; Li et al., 2012).

CAC is the most feared long-term intestinal complication of IBD, including UC (Peyrin-Biroulet et al., 2012). Especially, patients with early-onset UC face higher risk of developing not only CAC but also various kinds of cancers (Olen et al., 2017). It is frustrating that despite of this, there is no effective way but surveillance colonoscopy with biopsies to counterstrike this risk (Yu et al., 2016). Our study now showed that oral administration of montmorillonite can prevent ELF4 downregulation in DSS-induced colitis and lower the risk of CAC in mice models and possibly in patients with UC. Although further study including prospective clinical study should be conducted, our data showed hope for safe, effective, and economical treatment in CAC prevention.

In summary, we have shown that *Elf4*$^{-/-}$ mice are hyper-susceptible to CAC, and patients with UC show ELF4 deficiency in the colon mucosa. ELF4 intrinsically regulates a set of DDR machinery components to keep the epithelial genome stable in response to various genotoxic stimulations. Meanwhile, ELF4 is critical for mucin and REG protein expression, which form a physical barrier to protect intestinal epithelia

from mutagen attacks. ELF4 deficiency is an oncogenic hit and might be caused by a recently proposed process of epigenetic priming (Vicente-Duenas et al., 2018), which can be prevented by administration of montmorillonite powder, although further prospective clinical study should be done to fully explore its cancer prevention potential. These findings should inspire future clinical investigation and might change the paradigm of UC treatment.

Limitations of the study

The mechanisms of ELF4 suppression proposed in this manuscript are mostly based on preclinical animal model of UC and CAC, and further studies are needed to determine if those are clinically meaningful. The most exciting finding in this study is that the use of montmorillonite powder prevented ELF4 downregulation and delayed CAC development in some patients; however, the sample size is too small to propose a promising and novel cancer prevention strategy. ELF4 suppression is confirmed in patient cohorts from GEO but only in a small number of our patients. More well-cryopreserved clinical tissues should be collected for qPCR and western blot (WB) to confirm our finding in animal models.

Resource availability

Lead contact

Further information and requests for resources and reagents should be directed to and will be fulfilled by the lead contact, Fuping You, Ph.D (fupingyou@hsc.pku.edu.cn).

Material availability

This study did not generate new unique reagents.

Data and code availability

The RNA-seq data that support the findings in this study have been deposited in the GEO database with the accession codes GSE121305 and GSE164355. Raw data from Figures 1, 2, 3, 4, 5, and 6 and Figures S1, S3, S4, S6, and S7 were deposited on Mendeley at [https://data.mendeley.com/datasets/f734b48h8h/draft?a=8e1387fe-44f3-4551-b7d6-df1cd3986c6f].

METHODS

All methods can be found in the accompanying Transparent Methods supplemental file.

SUPPLEMENTAL INFORMATION

Supplemental information can be found online at https://doi.org/10.1016/j.isci.2021.102169.

ACKNOWLEDGMENTS

We thank the patients for their understanding and cooperation. This work was supported by the National Key Research and Development Program of China (2016YFA0500302 to F.Y.) and the National Natural Science Foundation of China (31570891 and 31872736 to F.Y., as well as 81871160 to M.L.).

AUTHOR CONTRIBUTIONS

H.D. conceived the project; designed, executed, and interpreted the animal studies; analyzed data and wrote the manuscript. H.X. and TT.L. executed most animal and cellular studies. Y.L. and J.L. collected clinical samples and analyzed patient information. B.X. performed comet tail assays. J.X. and T.L. executed animal studies related to infection mice models. L.C. and S.L. executed mass spectrometry assays. S.L. and P.W. constructed ELF4 knockdown and knockout plasmids. D.W., Z.Z., and Y.L. helped with lentivirus packaging. X.G. critically discussed ILC data. A.W. and M.L. conceived the project, critically discussed data, provided reagents, and revised manuscript. F.Y. conceived the project, designed and interpreted the animal and cellular studies, and wrote the manuscript.

DECLARATION OF INTERESTS

The authors declare no competing interests.

Received: September 12, 2020
Revised: January 12, 2021
Accepted: February 5, 2021
Published: March 19, 2021

REFERENCES

Akhtar-Zaidi, B., Cowper-Sal-lari, R., Corradin, O., Saiakhova, A., Bartels, C.F., Balasubramanian, D., Myeroff, L., Lutterbaugh, J., Jarrar, A., Kalady, M.F., et al. (2012). Epigenomic enhancer profiling defines a signature of colon cancer. Science *336*, 736–739.

Bischoff, S.C., Barbara, G., Buurman, W., Ockhuizen, T., Schulzke, J.D., Serino, M., Tilg, H., Watson, A., and Wells, J.M. (2014). Intestinal permeability–a new target for disease prevention and therapy. BMC Gastroenterol. *14*, 189.

Colotta, F., Allavena, P., Sica, A., Garlanda, C., and Mantovani, A. (2009). Cancer-related inflammation, the seventh hallmark of cancer: links to genetic instability. Carcinogenesis *30*, 1073–1081.

Conrad, K., Roggenbuck, D., and Laass, M.W. (2014). Diagnosis and classification of ulcerative colitis. Autoimmun. Rev. *13*, 463–466.

Curina, A., Termanini, A., Barozzi, I., Prosperini, E., Simonatto, M., Polletti, S., Silvola, A., Soldi, M., Austenaa, L., Bonaldi, T., et al. (2017). High constitutive activity of a broad panel of housekeeping and tissue-specific cis-regulatory elements depends on a subset of ETS proteins. Genes Dev. *31*, 399–412.

Dupont, C., Foo, J.L., Garnier, P., Moore, N., Mathiex-Fortunet, H., and Salazar-Lindo, E.; Peru, and Malaysia Diosmectite Study, G. (2009). Oral diosmectite reduces stool output and diarrhea duration in children with acute watery diarrhea. Clin. Gastroenterol. Hepatol. *7*, 456–462.

Dupont, C., and Vernisse, B. (2009). Anti-diarrheal effects of diosmectite in the treatment of acute diarrhea in children: a review. Paediatr. Drugs *11*, 89–99.

Eaden, J.A., Abrams, K.R., and Mayberry, J.F. (2001). The risk of colorectal cancer in ulcerative colitis: a meta-analysis. Gut *48*, 526–535.

Ekbom, A., Helmick, C., Zack, M., and Adami, H.O. (1990). Ulcerative colitis and colorectal cancer. A population-based study. New Engl. J. Med. *323*, 1228–1233.

Emmett, R.A., Davidson, K.L., Gould, N.J., and Arasaradnam, R.P. (2017). DNA methylation patterns in ulcerative colitis-associated cancer: a systematic review. Epigenomics *9*, 1029–1042.

Foran, E., Garrity-Park, M.M., Mureau, C., Newell, J., Smyrk, T.C., Limburg, P.J., and Egan, L.J. (2010). Upregulation of DNA methyltransferase-mediated gene silencing, anchorage-independent growth, and migration of colon cancer cells by interleukin-6. Mol. Cancer Res. *8*, 471–481.

Fouad, Y.A., and Aanei, C. (2017). Revisiting the hallmarks of cancer. Am. J. Cancer Res. *7*, 1016–1036.

Gagné, J.P., Hunter, J.M., Labrecque, B., Chabot, B., and Poirier, G.G. (2003). A proteomic approach to the identification of heterogeneous nuclear ribonucleoproteins as a new family of poly(ADP-ribose)-binding proteins. Biochem. J. *371*, 331–340.

Gkouskou, K.K., Ioannou, M., Pavlopoulos, G.A., Georgila, K., Siganou, A., Nikolaidis, G., Kanellis, D.C., Moore, S., Papadakis, K.A., Kardassis, D., et al. (2016). Apolipoprotein A-I inhibits experimental colitis and colitis-propelled carcinogenesis. Oncogene *35*, 2496–2505.

Gonzalez, R., de Medina, F.S., Martinez-Augustin, O., Nieto, A., Galvez, J., Risco, S., and Zarzuelo, A. (2004). Anti-inflammatory effect of diosmectite in hapten-induced colitis in the rat. Br. J. Pharmacol. *141*, 951–960.

Grivennikov, S.I. (2013). Inflammation and colorectal cancer: colitis-associated neoplasia. Semin. Immunopathol *35*, 229–244.

Grivennikov, S.I., and Cominelli, F. (2016). Colitis-associated and sporadic colon cancers: different diseases, different mutations? Gastroenterology *150*, 808–810.

Hanahan, D., and Weinberg, R.A. (2011). Hallmarks of cancer: the next generation. Cell *144*, 646–674.

Heazlewood, C.K., Cook, M.C., Eri, R., Price, G.R., Tauro, S.B., Taupin, D., Thornton, D.J., Png, C.W., Crockford, T.L., Cornall, R.J., et al. (2008). Aberrant mucin assembly in mice causes endoplasmic reticulum stress and spontaneous inflammation resembling ulcerative colitis. PLoS Med. *5*, e54.

Hussain, S.P., Hofseth, L.J., and Harris, C.C. (2003). Radical causes of cancer. Nat. Rev. Cancer *3*, 276–285.

Jess, T., Rungoe, C., and Peyrin-Biroulet, L. (2012). Risk of colorectal cancer in patients with ulcerative colitis: a meta-analysis of population-based cohort studies. Clin. Gastroenterol. Hepatol. *10*, 639–645.

Lee, P.H., Puppi, M., Schluns, K.S., Yu-Lee, L.Y., Dong, C., and Lacorazza, H.D. (2014). The transcription factor E74-like factor 4 suppresses differentiation of proliferating CD4+ T cells to the Th17 lineage. J. Immunol. *192*, 178–188.

Li, L.C., and Dahiya, R. (2002). MethPrimer: designing primers for methylation PCRs. Bioinformatics *18*, 1427–1431.

Li, Y., Deuring, J., Peppelenbosch, M.P., Kuipers, E.J., de Haar, C., and van der Woude, C.J. (2012). IL-6-induced DNMT1 activity mediates SOCS3 promoter hypermethylation in ulcerative colitis-related colorectal cancer. Carcinogenesis *33*, 1889–1896.

Long, A.G., Lundsmith, E.T., and Hamilton, K.E. (2017). Inflammation and colorectal cancer. Curr. Colorectal Cancer Rep. *13*, 341–351.

Loonen, L.M., Stolte, E.H., Jaklofsky, M.T., Meijerink, M., Dekker, J., van Baarlen, P., and Wells, J.M. (2014). REG3gamma-deficient mice have altered mucus distribution and increased mucosal inflammatory responses to the microbiota and enteric pathogens in the ileum. Mucosal Immunol. *7*, 939–947.

Mah, L.J., El-Osta, A., and Karagiannis, T.C. (2010). gammaH2AX: a sensitive molecular marker of DNA damage and repair. Leukemia *24*, 679–686.

Malewicz, M., and Perlmann, T. (2014). Function of transcription factors at DNA lesions in DNA repair. Exp. Cell. Res. *329*, 94–100.

Martini, E., Krug, S.M., Siegmund, B., Neurath, M.F., and Becker, C. (2017). Mend your fences: the epithelial barrier and its relationship with mucosal immunity in inflammatory bowel disease. Cell Mol. Gastroenterol. Hepatol. *4*, 33–46.

Mei, S., Qin, Q., Wu, Q., Sun, H., Zheng, R., Zang, C., Zhu, M., Wu, J., Shi, X., Taing, L., et al. (2017). Cistrome Data Browser: a data portal for ChIP-Seq and chromatin accessibility data in human and mouse. Nucleic Acids Res. *45*, D658–D662.

Meira, L.B., Bugni, J.M., Green, S.L., Lee, C.W., Pang, B., Borenshtein, D., Rickman, B.H., Rogers, A.B., Moroski-Erkul, C.A., McFaline, J.L., et al. (2008). DNA damage induced by chronic inflammation contributes to colon carcinogenesis in mice. J. Clin. Invest. *118*, 2516–2525.

Mielke, L.A., Jones, S.A., Raverdeau, M., Higgs, R., Stefanska, A., Groom, J.R., Misiak, A., Dungan, L.S., Sutton, C.E., Streubel, G., et al. (2013). Retinoic acid expression associates with enhanced IL-22 production by γδ T cells and innate lymphoid cells and attenuation of intestinal inflammation. J. Exp. Med. *210*, 1117–1124.

Moyer, M.P., Manzano, L.A., Merriman, R.L., Stauffer, J.S., and Tanzer, L.R. (1996). NCM460, a normal human colon mucosal epithelial cell line. Vitro Cell Dev. Biol. Anim. *32*, 315–317.

Netea, M.G., Joosten, L.A., Latz, E., Mills, K.H., Natoli, G., Stunnenberg, H.G., O'Neill, L.A., and Xavier, R.J. (2016). Trained immunity: a program of innate immune memory in health and disease. Science *352*, aaf1098.

Ng, S.C., Shi, H.Y., Hamidi, N., Underwood, F.E., Tang, W., Benchimol, E.I., Panaccione, R., Ghosh, S., Wu, J.C.Y., Chan, F.K.L., et al. (2018). Worldwide incidence and prevalence of inflammatory bowel disease in the 21st century: a systematic review of population-based studies. Lancet *390*, 2769–2778.

Nie, J., Sakamoto, S., Song, D., Qu, Z., Ota, K., and Taniguchi, T. (1998). Interaction of Oct-1 and automodification domain of poly(ADP-ribose) synthetase. FEBS Lett. *424*, 27–32.

Okayasu, I., Yamada, M., Mikami, T., Yoshida, T., Kanno, J., and Ohkusa, T. (2002). Dysplasia and carcinoma development in a repeated dextran sulfate sodium-induced colitis model. J. Gastroenterol. Hepatol. *17*, 1078–1083.

Olen, O., Askling, J., Sachs, M.C., Frumento, P., Neovius, M., Smedby, K.E., Ekbom, A., Malmborg, P., and Ludvigsson, J.F. (2017). Childhood onset inflammatory bowel disease and risk of cancer: a Swedish nationwide cohort study 1964-2014. BMJ *358*, j3951.

Peyrin-Biroulet, L., Lepage, C., Jooste, V., Gueant, J.L., Faivre, J., and Bouvier, A.M. (2012). Colorectal cancer in inflammatory bowel diseases: a population-based study (1976-2008). Inflamm. Bowel Dis. *18*, 2247–2251.

Ray Chaudhuri, A., and Nussenzweig, A. (2017). The multifaceted roles of PARP1 in DNA repair and chromatin remodelling. Nat. Rev. Mol. Cell Biol. *18*, 610–621.

Roszkowski, K., Jozwicki, W., Blaszczyk, P., Mucha-Malecka, A., and Siomek, A. (2011). Oxidative damage DNA: 8-oxoGua and 8-oxodG as molecular markers of cancer. Med. Sci. Monit. *17*, CR329–333.

Sanford, K.K., Price, F.M., Brodeur, C., Makrauer, F.L., and Parshad, R. (1997). Deficient DNA repair in chronic ulcerative colitis. Cancer Detect Prev. *21*, 540–545.

Sashida, G., Bae, N., Di Giandomenico, S., Asai, T., Gurvich, N., Bazzoli, E., Liu, Y., Huang, G., Zhao, X., Menendez, S., et al. (2011). The mef/elf4 transcription factor fine tunes the DNA damage response. Cancer Res. *71*, 4857–4865.

Sonnenberg, G.F., and Artis, D. (2015). Innate lymphoid cells in the initiation, regulation and resolution of inflammation. Nat. Med. *21*, 698–708.

Suico, M.A., Shuto, T., and Kai, H. (2017). Roles and regulations of the ETS transcription factor ELF4/MEF. J. Mol. Cell Biol. *9*, 168–177.

Terzic, J., Grivennikov, S., Karin, E., and Karin, M. (2010). Inflammation and colon cancer. Gastroenterology *138*, 2101–2114 e2105.

Uhlen, M., Bjorling, E., Agaton, C., Szigyarto, C.A., Amini, B., Andersen, E., Andersson, A.C., Angelidou, P., Asplund, A., Asplund, C., et al. (2005). A human protein atlas for normal and cancer tissues based on antibody proteomics. Mol. Cell Proteomics *4*, 1920–1932.

Ungaro, R., Mehandru, S., Allen, P.B., Peyrin-Biroulet, L., and Colombel, J.F. (2017). Ulcerative colitis. Lancet *389*, 1756–1770.

Velcich, A., Yang, W., Heyer, J., Fragale, A., Nicholas, C., Viani, S., Kucherlapati, R., Lipkin, M., Yang, K., and Augenlicht, L. (2002). Colorectal cancer in mice genetically deficient in the mucin Muc2. Science *295*, 1726–1729.

Vicente-Duenas, C., Hauer, J., Cobaleda, C., Borkhardt, A., and Sanchez-Garcia, I. (2018). Epigenetic priming in cancer initiation. Trends Cancer *4*, 408–417.

Wei, G.H., Badis, G., Berger, M.F., Kivioja, T., Palin, K., Enge, M., Bonke, M., Jolma, A., Varjosalo, M., Gehrke, A.R., et al. (2010). Genome-wide analysis of ETS-family DNA-binding in vitro and in vivo. EMBO J. *29*, 2147–2160.

Wells, J.M., Brummer, R.J., Derrien, M., MacDonald, T.T., Troost, F., Cani, P.D., Theodorou, V., Dekker, J., Meheust, A., de Vos, W.M., et al. (2017). Homeostasis of the gut barrier and potential biomarkers. Am. J. Physiol. Gastrointest. Liver Physiol. *312*, G171–G193.

You, F., Wang, P., Yang, L., Yang, G., Zhao, Y.O., Qian, F., Walker, W., Sutton, R., Montgomery, R., Lin, R., et al. (2013). ELF4 is critical for induction of type I interferon and the host antiviral response. Nat. Immunol. *14*, 1237–1246.

Yu, J.X., East, J.E., and Kaltenbach, T. (2016). Surveillance of patients with inflammatory bowel disease. Best Pract. Res. Clin. Gastroenterol. *30*, 949–958.

Zhao, J., Ng, S.C., Lei, Y., Yi, F., Li, J., Yu, L., Zou, K., Dan, Z., Dai, M., Ding, Y., et al. (2013). First prospective, population-based inflammatory bowel disease incidence study in mainland of China: the emergence of "western" disease. Inflamm. Bowel Dis. *19*, 1839–1845.

iScience, Volume *24*

Supplemental information

Suppression of ELF4 in ulcerative colitis predisposes host to colorectal cancer

Hongqiang Du, Huawei Xia, Tongtong Liu, Yingjie Li, Jilong Liu, Bingteng Xie, Jingxuan Chen, Tong Liu, Lili Cao, Shengde Liu, Siji Li, Peiyan Wang, Dandan Wang, Zeming Zhang, Yunfei Li, Xiaohuan Guo, Aiwen Wu, Mo Li, and Fuping You

Supplementary Figure 1: ELF4 is highly expressed in colon epithelial, related to Figure 1.

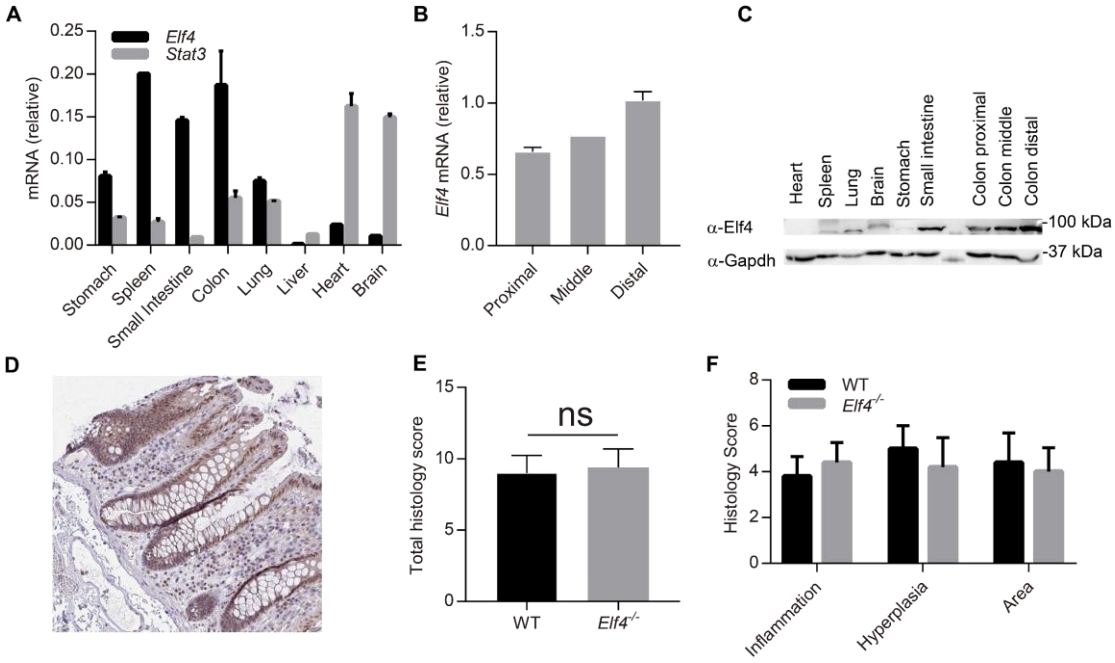

A-C, Expression profile of *Elf4* and *Stat3* in mouse analyzed by RT-qPCR (**A, B**) and western blot (**C**). Proximal, proximal section of colon; Middle, middle section of colon; Distal, distal section of colon. Data represent three technical repeats in all RT-qPCR assay. n=3.

D, Immunohistochemistry for ELF4 in healthy human colon tissue biopsy from protein atlas (available from www.proteinatlas.org; https://www.proteinatlas.org/ENSG00000102034-ELF4/tissue/colon#img).

E and **F**, H&E stained sections were scored for inflammation, ulceration, hyperplasia, and inflamed area. WT, n=10; Elf4 − / − , n=7. NS, not significant. Two-sided Student' s t-test, data are represented as mean ± SEM.

Supplementary Figure 2: ELF4 deficiency is prevalent in UC patients and mice models, related to Figure 2.

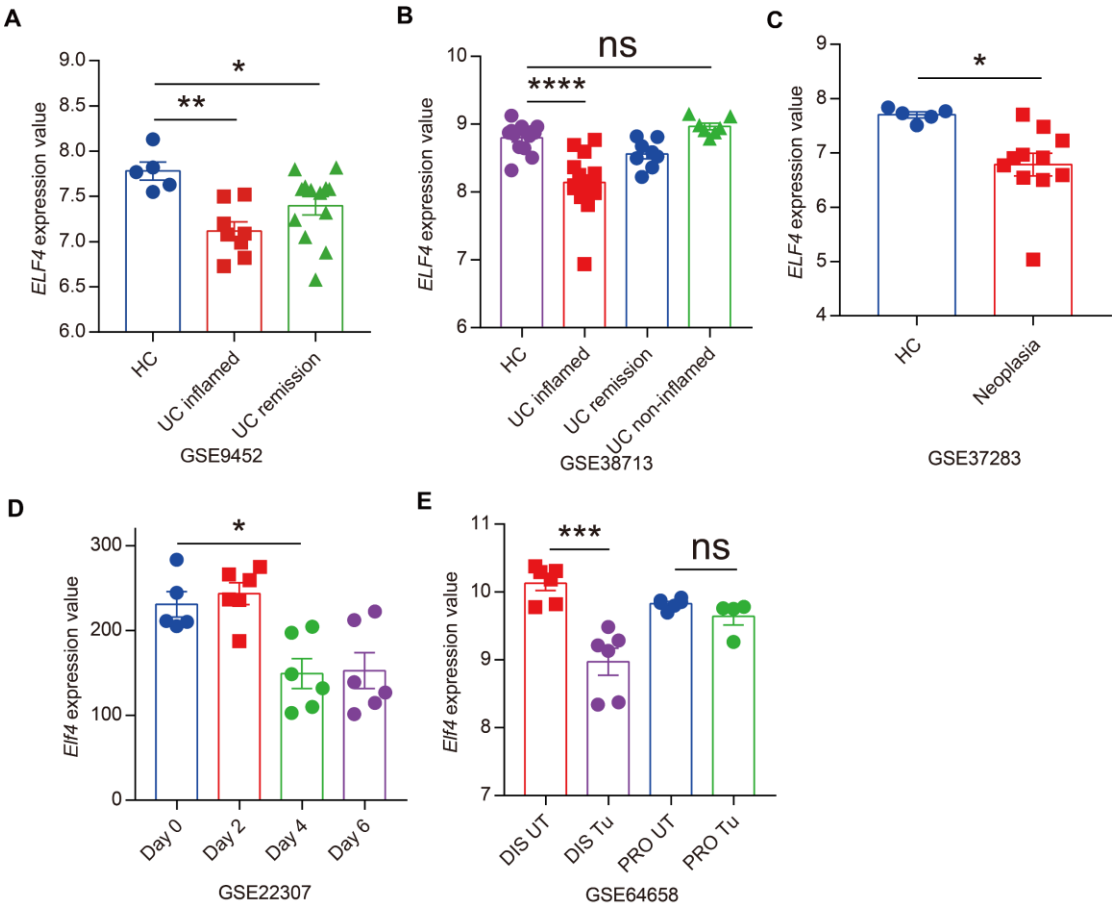

A, Comparison of *ELF4* among 5 healthy controls, 8 active UC and 13 inactive UC patients. HC, healthy controls; UC inflamed, active UC; UC remission, inactive UC. ***P*= 0.0011, **P*= 0.0468. Raw data were derived from GSE9452. Unpaired two-sided Student' s t-test, data are represented as mean ± SEM.

B, Comparison of *ELF4* among 13 healthy controls, 15 involved active UC, 8 inactive UC, 7 non-involved active UC patients. UC non-inflamed, non-involved active UC. *****P*= 3.59×10^{-5}. NS, not significant. Raw data were derived from GSE38713. Unpaired two-sided Student' s t-test, data are represented as mean ± SEM.

C, Comparison of *ELF4* between 5 healthy controls and 11 UC patients with neoplasia.

HC, healthy controls; Neoplasia, non-dysplastic tissue from UC patients harboring remote neoplasia. *P= 0.0123. Raw data were derived from GSE37283. Unpaired two-sided Student' s t-test, data are represented as mean ± SEM.

D, Temporal expression of *Elf4* during the development of acute colitis in DSS induced mice model. Day 0, n=5; Day2, n=6; Day 4, n=6; Day 6, n=6. **P= 0.0072. Raw data were derived from GSE22307. Unpaired two-sided Student' s t-test, data are represented as mean ± SEM.

E, Comparison of *Elf4* in different location of colon between control and CAC mice. DIS UT, distal colon tissue of untreated mice, n=6; DIS Tu, distal colon tumor tissue of CAC mice, n=6; PRO UT, proximal colon tissue of untreated mice, n=6; PRO Tu, proximal colon tumor of CAC mice, n=4. ***P= 0.0005. Raw data were derived from GSE64658. Unpaired two-sided Student' s t-test, data are represented as mean ± SEM.

Supplementary Figure 3: Elf4 deficiency leads to robust inflammatory response to DSS treatment, related to Figure 3.

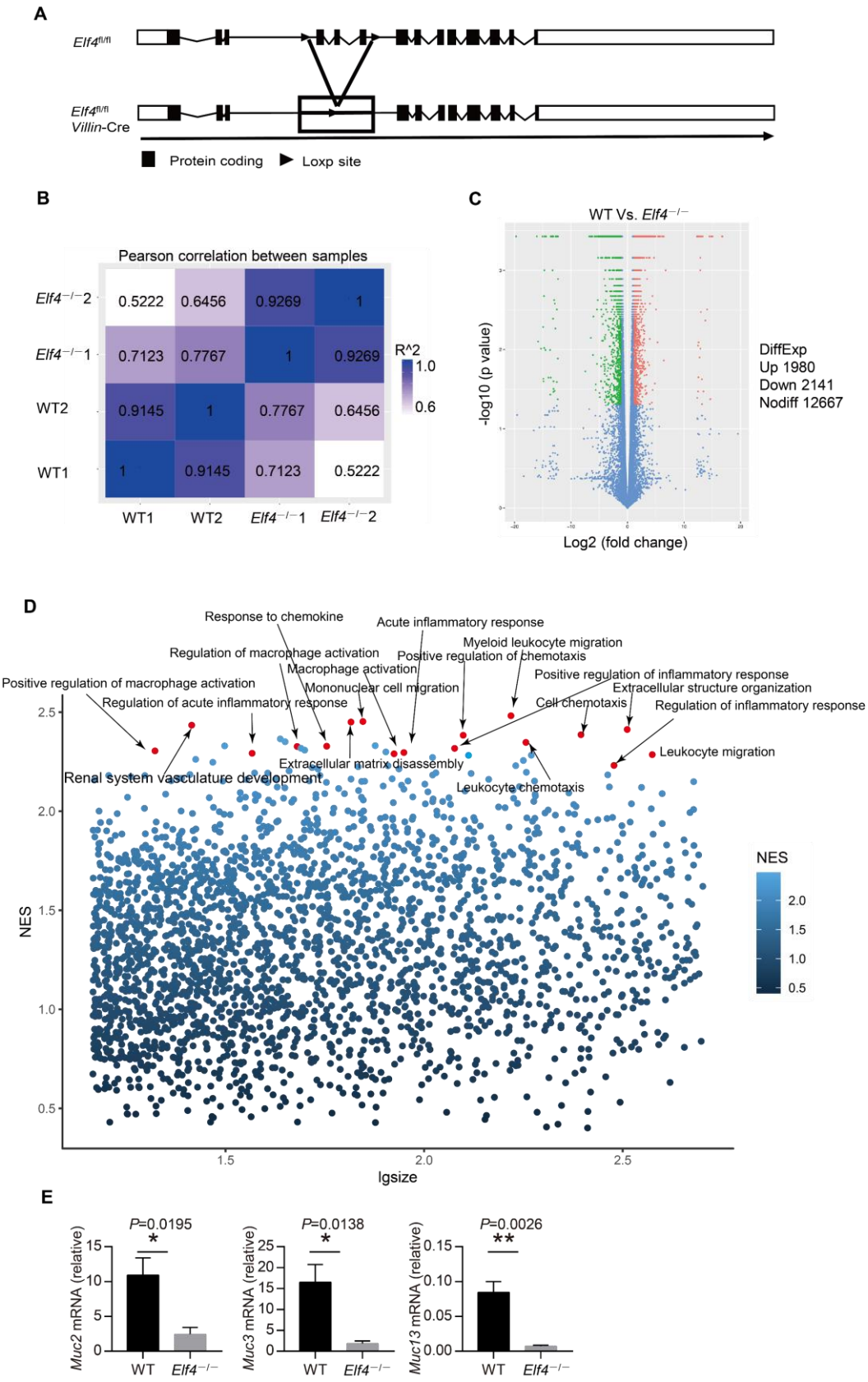

A, Schematic diagram of *Elf4*$^{fl/fl}$-Villin-Cre mice generation.

B, Heatmap showing Pearson correlation between DSS treated wild type and *Elf4*$^{-/-}$ mice samples.

C, Volcano plot indicating transcriptomic changes between DSS treated WT and *Elf4*$^{-/-}$ mice. Significantly upregulated (FC > 1, FDR-adj. p value < 0.05, red) and downregulated (FC<-1, FDR-adj. p value<0.05, green) genes are shown.

D, Gene set enrichment analysis (GSEA) of differentially expressed genes between DSS treated wide type (WT) and *Elf4*$^{fl/fl}$-Villin Cre mice, the top pathways enriched in *Elf4*$^{fl/fl}$-Villin Cre mice were marked. NES, normalized enrichment score, lgsize, logarithm of gene number contained in gene sets. n = 2 biological samples.

E, Comparison of indicated genes between DSS treated WT and *Elf4*$^{-/-}$ mice by RT-qPCR. WT, n=5; *Elf4*$^{-/-}$, n=5. **P* < 0.05, ***P* = 0.0026. Unpaired two-sided Student' s *t*-test, data are represented as mean ± SEM.

Supplementary Figure 4: ELF4 transcriptionally regulates DDR, related to Figure 4.

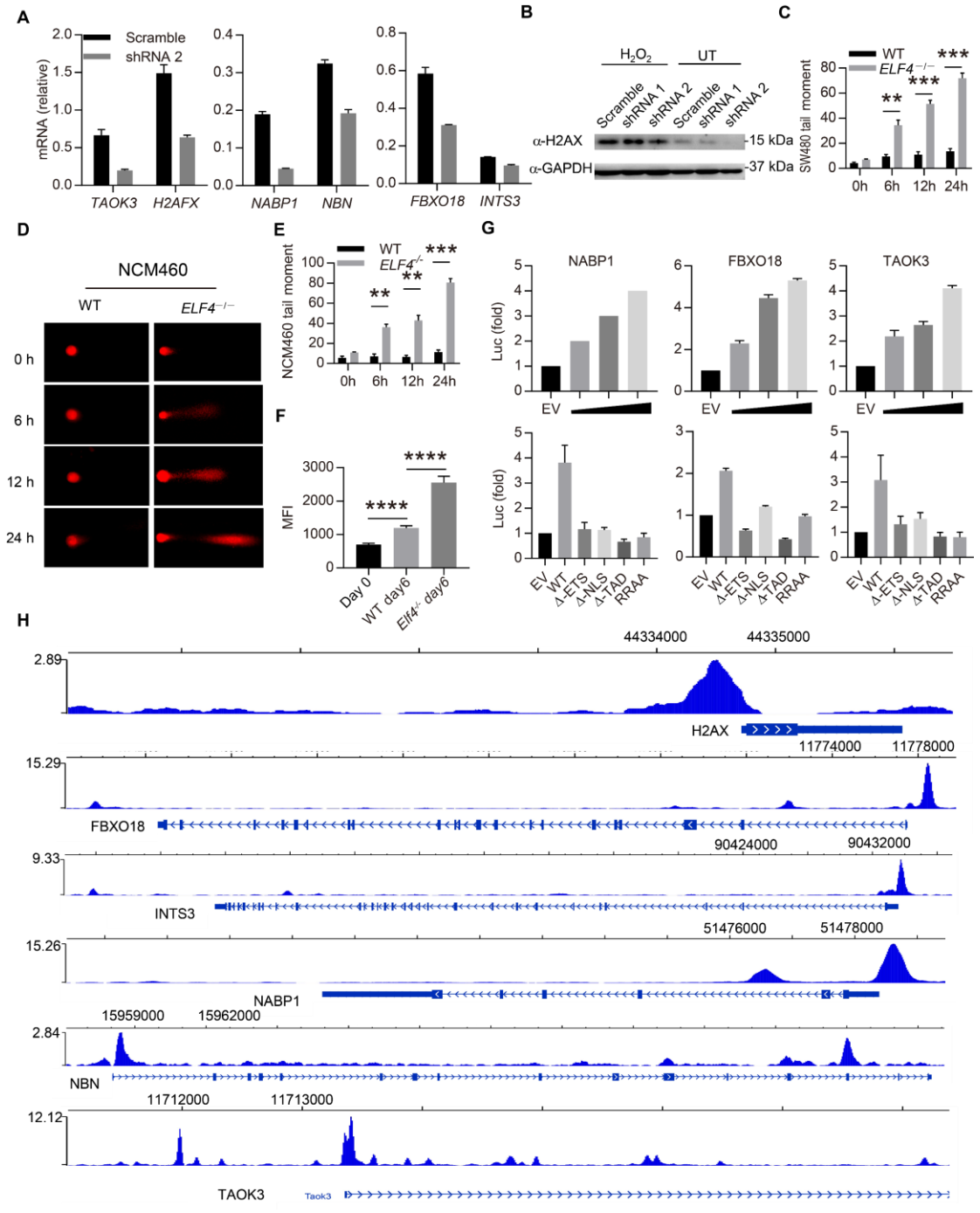

A, Comparison of indicated genes between H_2O_2 treated control and *ELF4* shRNA expressing SW480 cells by RT-qPCR, data are represented as mean ± SEM.

B, Comparison of H2AX between H_2O_2 treated control and *ELF4* shRNA expressing

SW480 cells by immunoblotting.

C, Tail moment analysis of the Comet assay in WT and *ELF4*$^{-/-}$ SW480 cells treated with H2O2 for indicated time. Data were pooled from three independent experiments. **P =0.0053, ***P < 0.001. Unpaired two-sided Student' s *t*-test, data are represented as mean ± SEM.

D, Representative images of Comet assay in WT and *ELF4*$^{-/-}$ NCM460 cells treated with H_2O_2 for indicated time.

E, Tail moment analysis of the Comet assay in WT and *ELF4*$^{-/-}$ NCM460 cells treated with H_2O_2 for indicated time. Data were pooled from three independent experiments. **P <0.01, ***P = 0.0001. Unpaired two-sided Student' s *t*-test, data are represented as mean ± SEM.

F, MFI analysis for 8-oxo-dG in the colon of indicated mice. MFI, mean fluorescence intensity. n=5, ****P < 0.0001. Unpaired two-sided Student' s *t*-test, data are represented as mean ± SEM.

G, Luciferase assay of HEK 293T cells transfected with indicated luciferase plasmids and various expression plasmids. Data were pooled from three independent experiments. WT, wild type ELF4, ΔETS (ELF4 without ETS domain), ΔNLS (ELF4 without the nuclear localization sequence), ΔTAD (ELF4 without transactivation domain), RRAA (ELF4-RRAA, RRAA indicates two arginines replaced by alanines) , data are represented as mean ± SEM.

H, Elf4 antibody binding peak in the promoters of *H2ax*, *Taok3*, *Nabp1*, *Nbn*, *Fbxo18* and *Inst3*. Raw data were derived from Cistrome database.

Supplementary Figure 5: ELF4 is epigenetically regulated during CAC, related to Figure 5.

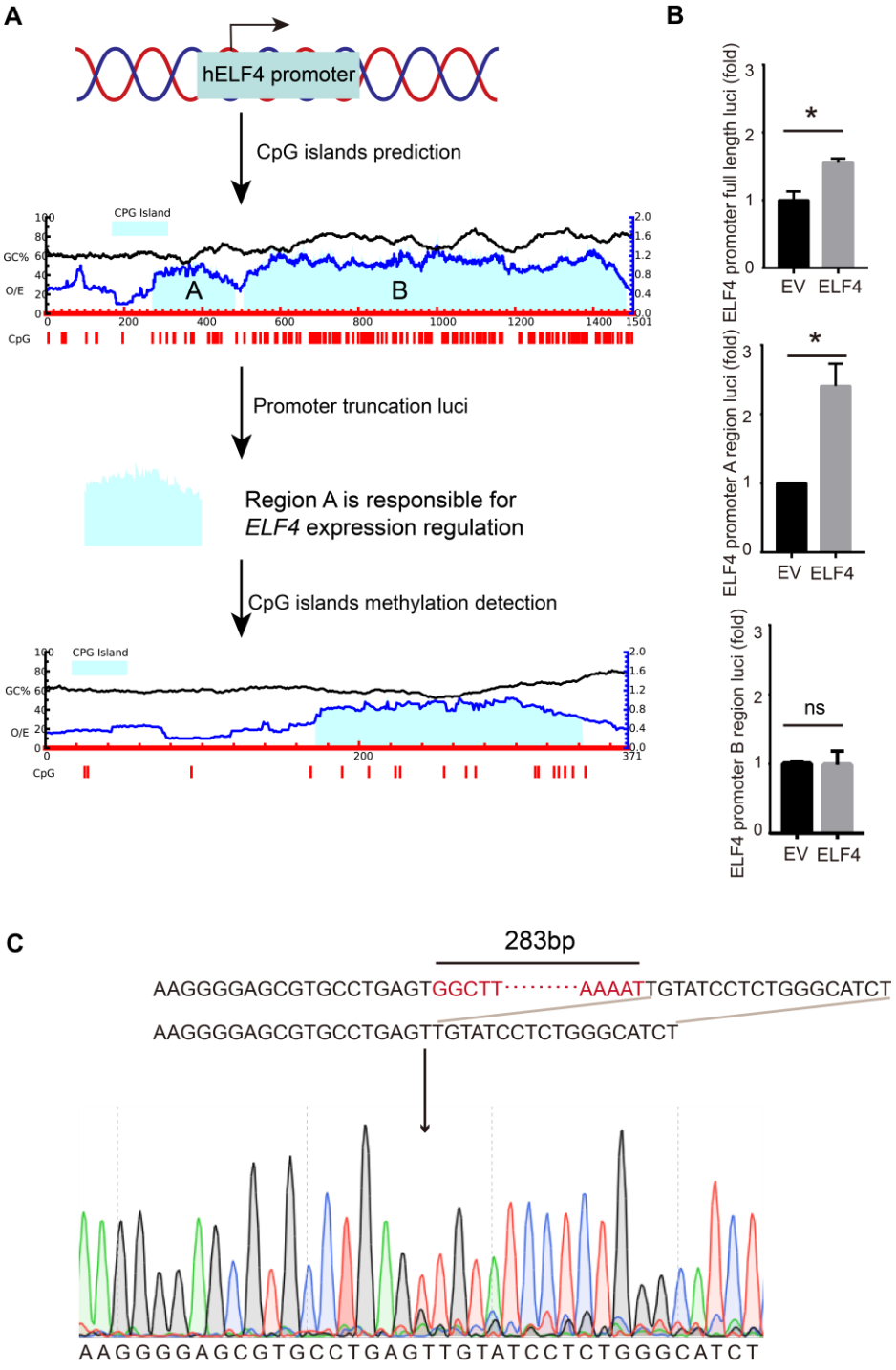

A, Schematic model of *ELF4* promoter region selection. And *ELF4* promoter CpG islands prediction by MethPrimer website. The red lines indicated CpG positions.

B, Luciferase assay of NCM460 cells transfected with *ELF4* promoter full length or

truncation luciferase plasmid and indicated expression plasmids. *$P < 0.01$, NS, not significant. Unpaired two-sided Student' s *t*-test, data are represented as mean ± SEM. Data were pooled from three independent experiments.

C, Schematic diagram of *ELF4* promoter region CpG1-11 deletion SW480 clone.

Supplementary Figure 6: Montmorillonite rescues *Elf4* expression, related to Figure 6.

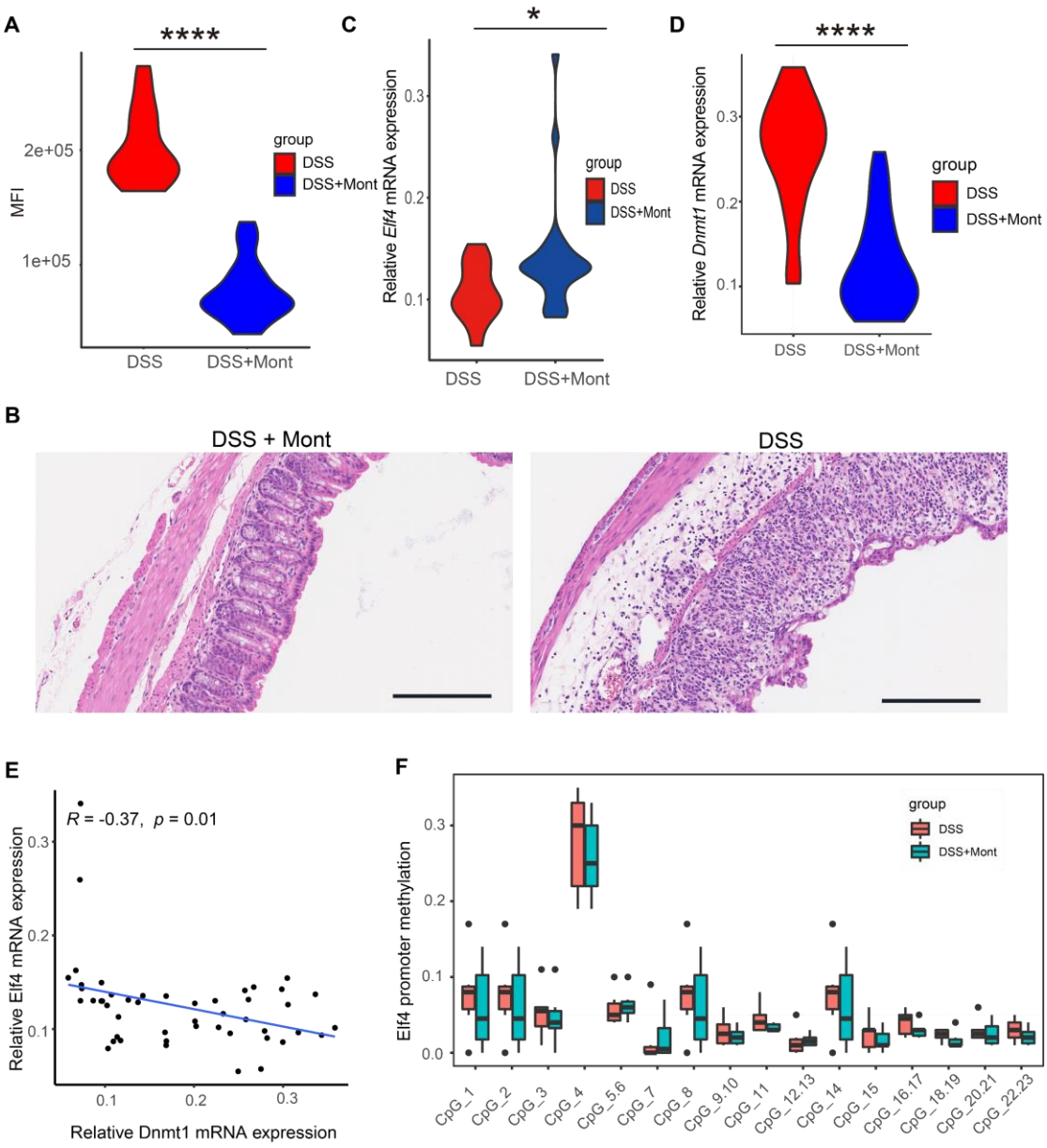

A, MFI analysis of 8-oxo-dG in the colon of indicated mice. MFI, mean fluorescence intensity. n=4, ****$P < 0.0001$. Unpaired two-sided Student' s *t*-test.

B, Representative H&E-stained colon sections images of indicated group. Scale bar: 200um.

C, *Elf4* mRNA expression of indicated mice. DSS group, n=11, DSS +Mont group, n=12. *$P = 0.0142$. Unpaired two-sided Student' s *t*-test.

D, *Dnmt1* mRNA expression of indicated mice. DSS group, n=11, DSS +Mont group, n=12. ****$P < 0.0001$. Unpaired two-sided Student' s *t*-test.

E, Correlation analysis of *Dnmt1* and *Elf4* mRNA expression of indicated mice. Pearson correlation analysis, R=-0.37, p=0.01.

F, Quantitative methylation analysis on each CpG site in a selected *Elf4* promoter region in mice inflammatory colon of indicated group. Methylation level 1 represents 100% methylated CpG dinucleotides on this site, data are represented as mean ± SEM.

Supplementary Figure 7: Oral administration of montmorillonite lowers risk of CAC development, related to Figure 6.

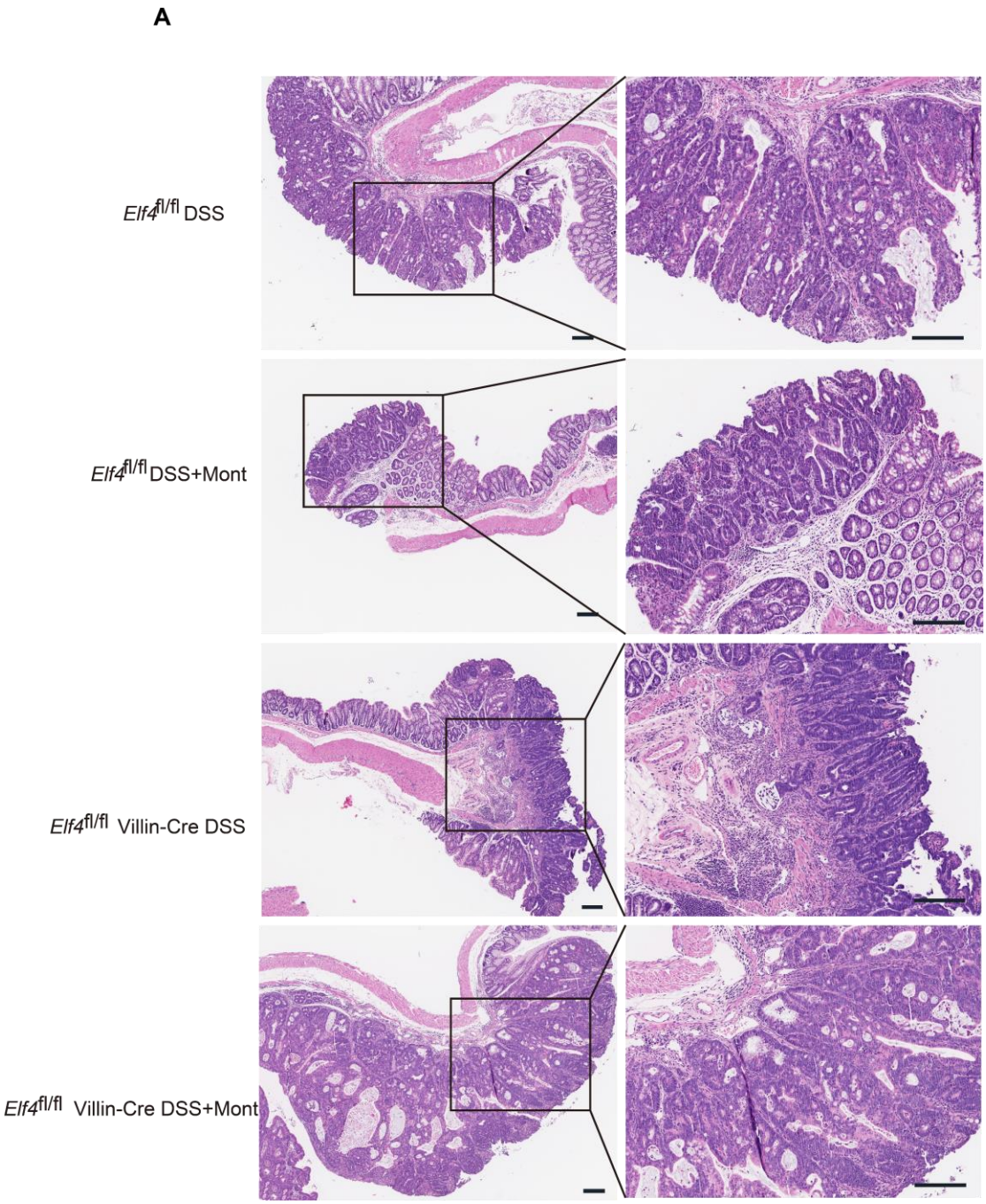

A, Representative colon H&E staining of indicated group. Scale bar: 200um.

Supplementary table 1. GEO dataset description, related to Figure 2.

Data set	GEO accession	Description	Contributors
hUC1	GSE9452	Analysis of colonic mucosa samples with or without signs of inflammation from patients with ulcerative colitis	Olsen J(Olsen et al., 2009)
hUC2	GSE38713	Analysis of colonic biopsies from patients with histologically active or inactive UC	Salas A(Planell et al., 2013)
hCAC	GSE37283	Gene Expression Changes in Non-Dysplastic Mucosa from Patients with Ulcerative Colitis Harboring Remote Neoplastic Lesions	Bissonnette M
mUC	GSE22307	Temporal genomewide expression profiling of DSS colitis	Kevil CG(Fang et al., 2011)
mCAC	GSE64658	Gene expression profiling of proximal versus distal mouse colon during AOM/DSS-induced colitis-associated carcinogenesis.	Pavlopoulos GA

Supplementary table 2. Description of enriched DDR pathway genes, related to Figure 4.

UniProt entry	Gene symble	Function
P27661	H2ax	Variant histone H2A which replaces conventional H2A in a subset of nucleosomes. Nucleosomes wrap and compact DNA into chromatin, limiting DNA accessibility to the cellular machineries which require DNA as a template. Histones thereby play a central role in transcription regulation, DNA repair, DNA replication and chromosomal stability. DNA accessibility is regulated via a complex set of post-translational modifications of histones, also called histone code, and nucleosome remodeling. Required for checkpoint-mediated arrest of cell cycle progression in response to low doses of ionizing radiation and for efficient repair of DNA double strand breaks (DSBs) specifically when modified by C-terminal phosphorylation.
Q8K2I9	Fbxo18	3'-5' DNA helicase and substrate-recognition component of the SCF(FBH1) E3 ubiquitin ligase complex that plays a key role in response to stalled/damaged replication forks (By similarity). Involved in genome maintenance by acting as an anti-recombinogenic helicase and preventing extensive strand exchange during homologous recombination: promotes RAD51 filament dissolution from stalled forks, thereby inhibiting homologous recombination and preventing excessive recombination. Also promotes cell death and DNA double-strand breakage in response to replication stress: together with MUS81, promotes the endonucleolytic DNA cleavage following prolonged replication stress via its helicase activity, possibly to eliminate cells with excessive replication stress. Plays a major role in remodeling of stalled DNA forks by catalyzing fork regression, in which the fork reverses and the two nascent DNA strands anneal. In addition to the helicase activity, also acts as the substrate-recognition component of the SCF(FBH1) E3 ubiquitin ligase complex, a complex that mediates ubiquitination of RAD51, leading to regulate RAD51 subcellular location.
Q8BYC6	Taok3	Serine/threonine-protein kinase that acts as a regulator of the p38/MAPK14 stress-activated MAPK cascade and of the MAPK8/JNK cascade. Acts as an activator of the p38/MAPK14 stress-activated MAPK cascade. In response to DNA damage, involved in the G2/M transition DNA damage checkpoint by activating the p38/MAPK14 stress-activated MAPK cascade, probably by mediating phosphorylation of upstream MAP2K3 and MAP2K6 kinases. Inhibits basal activity of MAPK8/JNK cascade and diminishes its activation in response epidermal growth factor (EGF)
Q9R207	Nbn	Component of the MRE11-RAD50-NBN (MRN complex) which plays a critical role in the cellular response to DNA damage and the

		maintenance of chromosome integrity. The complex is involved in double-strand break (DSB) repair, DNA recombination, maintenance of telomere integrity, cell cycle checkpoint control and meiosis. The complex possesses single-strand endonuclease activity and double-strand-specific 3'-5' exonuclease activity, which are provided by MRE11. RAD50 may be required to bind DNA ends and hold them in close proximity. NBN modulate the DNA damage signal sensing by recruiting PI3/PI4-kinase family members ATM, ATR, and probably DNA-PKcs to the DNA damage sites and activating their functions. It can also recruit MRE11 and RAD50 to the proximity of DSBs by an interaction with the histone H2AX. NBN also functions in telomere length maintenance by generating the 3' overhang which serves as a primer for telomerase dependent telomere elongation. NBN is a major player in the control of intra-S-phase checkpoint and there is some evidence that NBN is involved in G1 and G2 checkpoints. The roles of NBS1/MRN encompass DNA damage sensor, signal transducer, and effector, which enable cells to maintain DNA integrity and genomic stability. Forms a complex with RBBP8 to link DNA double-strand break sensing to resection. Enhances AKT1 phosphorylation possibly by association with the mTORC2 complex.
Q8BGW5	Nabp1	Component of the SOSS complex, a multiprotein complex that functions downstream of the MRN complex to promote DNA repair and G2/M checkpoint. In the SOSS complex, acts as a sensor of single-stranded DNA that binds to single-stranded DNA, in particular to polypyrimidines. The SOSS complex associates with DNA lesions and influences diverse endpoints in the cellular DNA damage response including cell-cycle checkpoint activation, recombinational repair and maintenance of genomic stability. Required for efficient homologous recombination-dependent repair of double-strand breaks (DSBs) and ATM-dependent signaling pathways
Q7TPD0	Ints3	Component of the Integrator (INT) complex. The Integrator complex is involved in the small nuclear RNAs (snRNA) U1 and U2 transcription and in their 3'-box-dependent processing. The Integrator complex is associated with the C-terminal domain (CTD) of RNA polymerase II largest subunit (POLR2A) and is recruited to the U1 and U2 snRNAs genes. Mediates recruitment of cytoplasmic dynein to the nuclear envelope, probably as component of the INT complex.By similarity Component of the SOSS complex, a multiprotein complex that functions downstream of the MRN complex to promote DNA repair and G2/M checkpoint. The SOSS complex associates with single-stranded DNA at DNA lesions and influences diverse endpoints in the cellular DNA damage response including cell-cycle checkpoint activation, recombinational repair and maintenance of genomic stability. The SOSS

	complex is required for efficient homologous recombination-dependent repair of double-strand breaks (DSBs) and ATM-dependent signaling pathways. In the SOSS complex, it is required for the assembly of the complex and for stabilization of the complex at DNA damage sites.

Supplementary table 3. ELF4 interacting proteins, related to Figure 4.

Accession	Description	Score	Coverage	# Peptides	# PSMs	MW [kDa]
Q99607	ETS-related transcription factor Elf-4 OS=Homo sapiens GN=ELF4 PE=1 SV=1 - [ELF4_HUMAN]	248.89	32.13	11	97	70.7
P09874	Poly [ADP-ribose] polymerase 1 OS=Homo sapiens GN=PARP1 PE=1 SV=4 - [PARP1_HUMAN]	183.75	34.81	28	62	113.0
P07437	Tubulin beta chain OS=Homo sapiens GN=TUBB PE=1 SV=2 - [TBB5_HUMAN]	158.09	39.19	13	50	49.6
P68371	Tubulin beta-4B chain OS=Homo sapiens GN=TUBB4B PE=1 SV=1 - [TBB4B_HUMAN]	147.82	42.92	14	45	49.8
P11142	Heat shock cognate 71 kDa protein OS=Homo sapiens GN=HSPA8 PE=1 SV=1 - [HSP7C_HUMAN]	141.08	34.98	20	45	70.9
Q9BVA1	Tubulin beta-2B chain OS=Homo sapiens GN=TUBB2B PE=1 SV=1 - [TBB2B_HUMAN]	131.15	42.92	14	40	49.9
Q13885	Tubulin beta-2A chain OS=Homo sapiens GN=TUBB2A PE=1 SV=1 - [TBB2A_HUMAN]	130.99	42.92	14	40	49.9
P0DMV8	Heat shock 70 kDa protein 1A OS=Homo sapiens GN=HSPA1A PE=1 SV=1 - [HS71A_HUMAN]	130.30	35.57	16	40	70.0
P68363	Tubulin alpha-1B chain OS=Homo sapiens GN=TUBA1B PE=1 SV=1 - [TBA1B_HUMAN]	100.57	48.78	16	37	50.1
P62701	40S ribosomal protein S4, X isoform OS=Homo sapiens GN=RPS4X PE=1 SV=2 - [RS4X_HUMAN]	93.09	42.21	11	31	29.6
P78527	DNA-dependent protein kinase catalytic subunit OS=Homo sapiens GN=PRKDC PE=1 SV=3 - [PRKDC_HUMAN]	92.20	5.40	17	29	468.8
P11021	78 kDa glucose-regulated protein OS=Homo sapiens GN=HSPA5 PE=1 SV=2 - [GRP78_HUMAN]	89.08	31.50	17	28	72.3
P35579	Myosin-9 OS=Homo sapiens GN=MYH9 PE=1 SV=4 - [MYH9_HUMAN]	87.72	13.32	19	27	226.4
P13010	X-ray repair cross-complementing protein 5 OS=Homo sapiens GN=XRCC5 PE=1 SV=3 - [XRCC5_HUMAN]	84.10	27.87	14	27	82.7
P12956	X-ray repair cross-complementing protein 6 OS=Homo sapiens GN=XRCC6 PE=1 SV=2 - [XRCC6_HUMAN]	71.69	30.21	15	25	69.8
P05141	ADP/ATP translocase 2 OS=Homo sapiens GN=SLC25A5 PE=1 SV=7 - [ADT2_HUMAN]	69.90	32.89	11	26	32.8
P15880	40S ribosomal protein S2 OS=Homo sapiens GN=RPS2 PE=1 SV=2 - [RS2_HUMAN]	69.80	24.23	7	25	31.3
P23396	40S ribosomal protein S3 OS=Homo sapiens GN=RPS3 PE=1 SV=2 - [RS3_HUMAN]	67.38	45.68	10	24	26.7
P19338	Nucleolin OS=Homo sapiens GN=NCL PE=1 SV=3 - [NUCL_HUMAN]	64.89	26.34	17	21	76.6
P33992	DNA replication licensing factor MCM5 OS=Homo sapiens GN=MCM5 PE=1 SV=5 - [MCM5_HUMAN]	62.13	26.43	13	19	82.2
Q00839	Heterogeneous nuclear ribonucleoprotein U OS=Homo sapiens GN=HNRNPU PE=1 SV=6 - [HNRPU_HUMAN]	61.40	22.30	15	20	90.5
P67809	Nuclease-sensitive element-binding protein 1 OS=Homo sapiens GN=YBX1 PE=1 SV=3 - [YBOX1_HUMAN]	60.76	32.72	7	17	35.9
P38646	Stress-70 protein, mitochondrial OS=Homo sapiens GN=HSPA9 PE=1 SV=2 - [GRP75_HUMAN]	58.81	28.13	15	19	73.6
P36578	60S ribosomal protein L4 OS=Homo sapiens GN=RPL4 PE=1 SV=5 - [RL4_HUMAN]	56.35	29.04	10	20	47.7
P62258	14-3-3 protein epsilon OS=Homo sapiens GN=YWHAE PE=1 SV=1 - [1433E_HUMAN]	52.78	51.76	11	18	29.2
Q9BUF5	Tubulin beta-6 chain OS=Homo sapiens GN=TUBB6 PE=1 SV=1 - [TBB6_HUMAN]	51.91	21.30	7	17	49.8
Q9BTE3	Mini-chromosome maintenance complex-binding protein OS=Homo sapiens GN=MCMBP PE=1 SV=2 - [MCMBP_H	51.75	17.91	10	17	72.9
P60709	Actin, cytoplasmic 1 OS=Homo sapiens GN=ACTB PE=1 SV=1 - [ACTB_HUMAN]	50.59	26.93	7	19	41.7
Q9NR30	Nucleolar RNA helicase 2 OS=Homo sapiens GN=DDX21 PE=1 SV=5 - [DDX21_HUMAN]	48.04	16.22	12	16	87.3
Q5T9A4	ATPase family AAA domain-containing protein 3B OS=Homo sapiens GN=ATAD3B PE=1 SV=1 - [ATD3B_HUMAN	45.98	18.36	10	15	72.5
Q9NVI7	ATPase family AAA domain-containing protein 3A OS=Homo sapiens GN=ATAD3A PE=1 SV=2 - [ATD3A_HUMAI	44.95	18.61	11	16	71.3
P39023	60S ribosomal protein L3 OS=Homo sapiens GN=RPL3 PE=1 SV=2 - [RL3_HUMAN]	44.54	27.30	11	16	46.1
P62829	60S ribosomal protein L23 OS=Homo sapiens GN=RPL23 PE=1 SV=1 - [RL23_HUMAN]	44.21	38.57	4	12	14.9
Q12906	Interleukin enhancer-binding factor 3 OS=Homo sapiens GN=ILF3 PE=1 SV=3 - [ILF3_HUMAN]	43.74	16.67	12	17	95.3
P10809	60 kDa heat shock protein, mitochondrial OS=Homo sapiens GN=HSPD1 PE=1 SV=2 - [CH60_HUMAN]	43.01	24.61	12	14	61.0
P17844	Probable ATP-dependent RNA helicase DDX5 OS=Homo sapiens GN=DDX5 PE=1 SV=1 - [DDX5_HUMAN]	42.96	20.36	13	19	69.1
Q08211	ATP-dependent RNA helicase A OS=Homo sapiens GN=DHX9 PE=1 SV=4 - [DHX9_HUMAN]	42.93	12.36	11	14	140.9
P12236	ADP/ATP translocase 3 OS=Homo sapiens GN=SLC25A6 PE=1 SV=4 - [ADT3_HUMAN]	42.87	36.58	12	19	32.8
P62241	40S ribosomal protein S8 OS=Homo sapiens GN=RPS8 PE=1 SV=2 - [RS8_HUMAN]	42.77	31.73	6	13	24.2
P31943	Heterogeneous nuclear ribonucleoprotein H OS=Homo sapiens GN=HNRNPH1 PE=1 SV=4 - [HNRH1_HUMAN]	42.49	15.59	5	11	49.2
P05388	60S acidic ribosomal protein P0 OS=Homo sapiens GN=RPLP0 PE=1 SV=1 - [RLA0_HUMAN]	40.64	39.43	9	15	34.3
P04264	Keratin, type II cytoskeletal 1 OS=Homo sapiens GN=KRT1 PE=1 SV=6 - [K2C1_HUMAN]	39.71	19.25	11	13	66.0
P42166	Lamina-associated polypeptide 2, isoform alpha OS=Homo sapiens GN=TMPO PE=1 SV=2 - [LAP2A_HUMAN]	39.39	23.63	10	11	75.4
P63267	Actin, gamma-enteric smooth muscle OS=Homo sapiens GN=ACTG2 PE=1 SV=1 - [ACTH_HUMAN]	38.37	17.29	5	13	41.8
P62753	40S ribosomal protein S6 OS=Homo sapiens GN=RPS6 PE=1 SV=1 - [RS6_HUMAN]	37.27	22.49	6	12	28.7
P08238	Heat shock protein HSP 90-beta OS=Homo sapiens GN=HSP90AB1 PE=1 SV=4 - [HS90B_HUMAN]	36.56	18.51	11	13	83.2

Supplementary table 4. Summary of patients in the retrospective study, related to Figure 6.

.

		gender	age	TNM diagnosis	immunohistochemical test
Never	P1	female	68	pT3N0M0	Cmet(1+), EGFR(3+), HER2(1+), Ki-67(+80%), MLH1(+50 ~ 75%), MSH2(+ > 75%), MSH6(+ > 75%), PMS2(+ > 75%)
	P2	female	56	pT3N2	Cmet(2+), EGFR(2+), HER2(0), Ki-67(90%+), MLH1(+), MSH2(+), MSH6(+), PMS2(+)
	P3	male	45	pT3N2b	Cmet(2+), EGFR(2+), HER2(1+), Ki-67(+50 ~ 75%), MLH1(+ > 75%), MSH2(+ > 75%), MSH6(+ > 75%), PMS2(+ > 75%)
	P4	male	38	pT3N0M0	C-met(2+)、EGFR(2+), HER-2(2+)
	P5	male	49	pT2N0M0	Cmet(+95%), EGFR(2+), HER2(0), Ki-67(+ > 75%), MLH1(+ > 75%), MSH2(+ > 75%), MSH6(+ > 75%), PMS2(+ > 75%)
	P6	male	34	pT3N1a	Cmet(+), EGFR(+), HER2(−), Ki-67(+25 ~ 50%), MLH1(+50 ~ 75%), MSH2(−), MSH6(−)
	P7	female	58	pT4bN2bM0	ND
	P8	female	43	pT4bN1M0	Cmet(+), EGFR(+), HER2(−), Ki-67(小于 25%)
	P9	male	60	pT4aN2bM1a	Cmet(+), EGFR(+), HER2(−), Ki-67(+50 ~ 75%), MLH1(+ > 75%), MSH2(+25 ~ 50%), MSH6(+ > 75%),
	P10	male	54	pT1N0	Cmet(+ > 75%), EGFR(+25 ~ 50%), HER2(−), Ki-67(+ < 25%), MLH1(−), MSH2(−), MSH6(−)
	P11	male	46	pT4N2M1	ND
	P12	male	55	pT4N1M0	ND
Occasionally	P13	male	40	pT3N0M0	Cmet(2+), EGFR(2+), HER2(1+), KI-67(+70%), MLH1(+), MSH2(+), MSH6(+), PMS2(+)
	P14	female	62	pT4aN0	Cmet(+), EGFR(−), HER2(2+), Ki-67(+ > 75%), MLH1(+25 ~ 50%), MSH2(+50 ~ 75%), MSH6(−)
	P15	male	54	pT1N0	Cmet(+), EGFR(−), HER2(3+), Ki-67(+25 ~ 50%), MLH1(+25 ~ 50%), MMP7(−), MSH2(+50 ~ 75%), MSH6(+ < 25%)
Regularly	P16	male	75	pT3N0M0	Cmet(+), EGFR(+), HER2(0), Ki-67(+50 ~ 75%), MLH1(+25 ~ 50%), MSH2(+50 ~ 75%), MSH6(+ > 75%), PMS2(+50 ~ 75%)
	P17	male	77	pT3N1b	Cmet(+90%), EGFR(3+), HER2(0), Ki-67(+50 ~ 75%), MLH1(+ > 75%), MSH2(+25 ~ 50%), MSH6(+ > 75%), PMS2(+ > 75%)
	P18	female	44	pT4bN1M0	ND

Transparent Methods

Mice

Elf4$^{-/-}$ mice on a C57BL/6J background have been described previously(You et al., 2013). Age and sex matched wild type mice were used. 8-10 weeks old mice were used. All mice were housed in pathogen-free facilities under 12-h light dark cycles with access to food and water ad libitum.

Cells, antibodies and reagents

HEK 293T (Human Embryonic Kidney 293 cells transformed by expression of the large T antigen from SV40) (ATCC, CRL-11268) were cultured in Dulbecco's modified Eagle medium (DMEM). SW480 (ATCC, CCL-228) and NCM460 (INCELL, CVCL-0460) were cultured in Roswell Park Memorial Institute (RPMI) 1640 medium supplemented with 10% fetal bovine serum (FBS), 1% P/S (100 IU/ml penicillin and 100 IU/ml streptomycin). Anti-GAPDH antibody (#10494-1-AP) and anti-ELF4 antibody (#16020-1-AP) were purchased from Proteintech. Anti-FLAG antibody (M2) and anti-HA antibody (H3663) were purchased from Sigma Aldrich. Anti-DNMT1 antibody (#ab188453), anti-DNA/RNA Damage antibody (#ab62623) and anti-H2AX antibody (#ab11175) were purchased from Abcam. Anti-PAR antibody (Trevigen, 4335). rIL-23 (#200-23-10) and rIL-6 (#200-06-5) was purchased from PeproTech. 5-Aza-2′-deoxycytidine (5-Aza-dC, #A3656) was purchased from Sigma Aldrich. Dextran sulfate sodium (DSS, #0216011080) was purchased from MP Biomedicals. Azoxymethane (AOM, #A5486) was purchased from Sigma Aldrich. Montmorillonite powder was bought from Beaufour-Ipsen (Tianjin) pharmaceutical company.

Generation of *Elf4*$^{fl/fl}$ mice

Elf4$^{fl/fl}$ mice on a C57BL/6J background were designed and generated by ShangHai Bangyao Biotech company using Crispr-Cas9 method. Exon 3 was chosen as target insertion site, Flox sequence was inserted by homologous recombination.

Elf4$^{fl/fl}$ mice were bred with Villin-Cre mice (T000142, Model Animal Research Center of Nanjing University) to generate *Elf4*$^{fl/fl}$- Villin-Cre mice.

Elf4$^{fl/fl}$ mice typing primers

primer	Sequence 5'——3'	Results
EfloxF	GCTGCAAAGCCTAATGACC	Wt：215bp；Mut：249bp
EfloxR	CTGAGAAGCCCACCCTACC	Hetero： 215bp+249bp

Villin-Cre mice typing primers

primer	Sequence 5'——3'	Results
VcreF	GCGCTGGAGTTTCAATACCGGAGAT	positive : 660bp
VcreR	CCAAAGGACCCGTTCGACAATACTCGTAA	

Patients and specimens

Patients with an established diagnosis of UC and healthy controls were included at the ChuiYangLiu Hospital affiliated to Tsinghua University. Healthy controls were those subjects undergoing colonoscopy for a screening for CRC, and who presented no lesions during examination. UC patients were aged between 18 and 65 years. Biopsies

were taken during routine colonoscopies, placed in RNA later RNA Stabilisation Reagent (Qiagen) and stored at −80°C.

We queried the pathology databases to identify all cases of bowel cancer seen at Peking University Cancer Hospital between 2013 and 2018 in which colitis as a clinical factor was indicated in the report. The medical records were reviewed. Pathology slides from all candidate cases were reviewed by a pathologist to confirm evidence of colitis and carcinoma, and the medical records were reviewed by a medical oncologist for the clinical history of IBD. 8 pairs of CAC tissue (adjacent and cancer tissue) were retrieved for DNA extraction and we were only able to extract total protein from 3 pairs due to sample quality and quantity.

Retrospective clinical study

We queried the surgery records database to identify all cases of colon cancer with a history of recurrent UC at Peking University Cancer Hospital between 2003 and 2018. A total of 18 CAC patients who provided Montmorillonite powder use history information, were included and their detailed clinical records were reviewed and related information was extracted, summarized, and analyzed.

Approval and consent for experiments

All procedures followed the Peking University Guidelines for "Using Animals in Intramural Research" and were approved by the ethics committee of Peking University Health Science Center (approved number LA2016240). For human specimens, Informed consent was provided by each subject before sample collection (according to

the Helsinki Declaration), and the study was approved by the ethics committee of Peking University Health Science Center.

Constructs (primer list)

pCMV7.1-3×FLAG-mELF4, pCMV7.1-3×FLAG-hELF4 wild type, deleted, truncated and point mutants were as described(You et al., 2013). pCMV7.1-3×FLAG-hPARP1 was cloned from HEK293T derived cDNA library. And then pCMV-3×HA-hELF4 and pCMV-3×HA-hPARP1 were subcloned from FLAG-tagged hELF4 and hPARP1. Promoters of H2AX, NABP1, FBXO18, TAOK3 and ELF4 were cloned into pGL3-Basic vector (Promega) with the following promoter regions: -2161 to 54 for H2AX, -1181 to -650 for NABP1, -256 to -153 for FBXO18, -1250 to -726 for TAOK3, -1292 to 7 for ELF4 full length, -1292 to -913 for ELF4 A region, -895 to 7 for ELF4 B region. Target sequences of shRNA against ELF4 and DNMT1 were selected from the Genetic Perturbation Platform at Broad Institute and cloned into PLKO.1 vector. All constructs were verified by sequencing. Related oligonucleotides were listed below:

primer name	**sequence (5'→3')**
H2AX pro F	CAATGCTCTTCCTATTAGCCACA
H2AX pro R	CTTCGTGCTGCCGAGTTTG
TAOK3 pro F	GCCAGGCAGGTCTGGAACCCTT
TAOK3 pro R	GCTTAACAAGGTTTCAGCAA
NABP1 pro F	ACCCAGCTCAGCCATTCTC
NABP1 pro R	CTGAGCAGGCAGGACTGCAA

FBXO18 pro F	CTCGACCGCCGCTGCTCCGC
FBXO18 pro R	CCTCACGCACTGTGGCGCTC
ELF4 pro full length F	GTGCCTGAGTGGCTTTCAAG
ELF4 pro full length R	GGAGAAGTGGAAGTTGAGC
ELF4 pro A region F	GTGCCTGAGTGGCTTTCAAG
ELF4 pro A region R	ACATTATTGAGCTCCTGGGGT
ELF4 pro B region F	CCAAAGGCGTCAAGCAAGTC
ELF4 pro B region R	GGAGAAGTGGAAGTTGAGC
eGFP shRNA	CCGGTACAACAGCCACAACGTCTATCTCGAGATAGACG TTGTGGCTGTTGTATTTTTG
DNMT1 shRNA 2#	CCGGGCCCAATGAGACTGACATCAACTCGAGTTGATGT CAGTCTCATTGGGCTTTTTG
ELF4 shRNA 1#	CCGGCGCGGAAGTCTTACTCAATATCTCGAGATATTGA GTAAGACTTCCGCGTTTTTG

ELF4 shRNA 2#	CCGGCCCTGATTTACTGCATCTGTACTCGAGTACAGATGCAGTAAATCAGGGTTTTTG
PARP1 shRNA	CCGGGCCCTTGGAAACATGTATGAACTCGAGTTCATACATGTTTCCAAGGGCTTTTTG

Coimmunoprecipitation

HEK293T cells seeded on 6-well plate (1×10^6 cells/well) were transfected with 1ug of empty plasmid or various expression plasmids. 24 hours after transfection, treated cells with or without H_2O_2 for 30 min, cells were lysed in lysis buffer (0.5% Triton-X-100, 20 mM HEPES (PH 7.4), 150 mM NaCl, 12.5 mM β-glycerolphosphate, 1.5 mM MgCl2, 2 mM EGTA, 10 mM NaF, 1 mM Na3VO4, 2 mM DTT) containing protease inhibitors. Lysates were centrifuged and the supernatant was incubated with anti-Flag antibodies at 4°C overnight. The next day, prewashed protein A/G beads (Pierce) were added and incubated at 4°C for 3 hours. The beads were washed with cold PBS 4 times and eluted with DTT-containing SDS sample buffer by boiling for 10 minutes for western blotting or mass spectrometry for interacting protein analysis.

Luciferase reporter assay

HEK 293T cells seeded on 24-well plates were transiently transfected with 50 ng of the luciferase reporter plasmid together with a total of 200 ng of various expression plasmids or empty control plasmids. As an internal control, 10 ng of pRL-TK was transfected simultaneously. Dual luciferase activity in the total cell lysates was quantified 24–36 h after transfection.

SW480 cells and NCM460 cells were plated in 24-well plates and transiently transfected with various ELF4 reporter plasmids. Luciferase activity was measured with the Dual-Luciferase Assay System (Promega) at 24 hours after transfection.

Immunofluorescence confocal microscopy

These experiments were performed as described(Maluach et al., 2017). Fluorescent images of all tissue sections were obtained using Nikon N-STORM system under a 40× objective.

Chromatin Immunoprecipitation (ChIP)

Approximately 10^7 cells were crosslinked with 1% formaldehyde at room temperature for 10 minutes, and the reaction was quenched with 0.125M glycine for 5 minutes. The cells were washed twice with PBS, then scrapped and pelleted at 2500 rpm for 5 minutes at 4 °C. After lysis and sonication, the purified DNA sizes were analyzed by 2% agarose gel electrophoresis. The majority of the sonicated DNA fragments were sheared to a size of around 200–600 bp. The sonicated chromatin was spun down at 12,000 rpm for 10 minutes at 4 °C to collect the chromatin. Then the soluble chromatin was incubated with 2-5 ug of anti-Flag antibodies or anti-$H_3K_4me_2$ antibodies and the mixture were rotated at 4 °C overnight. After incubation, pre-washed Protein G Dynabeads (10004d, Invitrogen) were added and incubated for 4 hours at 4ºC in a rotator. Then the magnetic Dynabeads were pelleted by placing the tubes in a magnetic rack and were washed for a total of five times: once with wash buffer A (20 mM Tris•HCl (pH 8.0), 500mM NaCl, 2 mM EDTA, 0.1% SDS, 1% Triton X-100); once

with wash buffer B (10 mMTris·HCl (pH 8.0), 250 mM LiCl, 1 mM EDTA, 1%NP-40); three times with wash buffer C (1 mM EDTA, 10 mM Tris•HCl (pH 8.0)).

After the last wash, beads were resuspended in 100 μl elution buffer (50 mM Tris•HCl (pH8.0), 10 mM EDTA, 1% SDS), followed by incubation at 65 °C overnight for reverse crosslink.

The next day, purify DNA with QIAquick PCR purification kit (Magen, D211102) and elute with 50 μl elution buffer. The extracted DNA was used for qRT-PCR with the specific PCR primers which were designed surrounding a specific region of 150–250 base pairs (bp) on target DNA.

The primer sequences were as following:

ChIP TAOK3 F	ATCAAACTGACGGCTGCTGAA
ChIP TAOK3 R	CAGGGACCACCATGTTAGAGC
ChIP FBXO18 F	GCTCGAAGGAACTCTGGGAAAG
ChIP FBXO18 R	TGACGGACGGCCACTAACG
ChIP INTS3 F	TACCACCCGACGGCATTT
ChIP INTS3 R	CGAGGCGATGAGGAAGGA
ChIP NABP1 F	TCACAGGTTCTAAACTCTACCGTTCC
ChIP NABP1 R	TCCCGTTCTCCACCCACTTC
ChIP NBN F	GGTGGAAGTGGAAAGGAAGG
ChIP NBN R	GATTTCACCTCGAAGTAAACTCA

ChIP IFNB1 F	TTGCTTTCCTTTGCTTTCTC
ChIP IFNB1 R	CCCACTTTCACTTCTCCCTT
ChIP ELF4 F	CCCAAAGGCGTCAAGCAAGTC
ChIP ELF4 R	CGGTGCGAAGCCCCCATACAA
ChIP Elf4 F	CAGCGTGACTTCACTGCTTCCC
ChIP Elf4 R	CTCCCAGCCCCTCCAACTTTCC

Flow cytometry

Isolation of Intestinal LPLs was as reported(Qiu et al., 2012). Single-cell suspensions or stimulated cells were first incubated for 10 min with anti-CD16/32 (2.4G2, Biolegend) for blockade of Fc receptors. Cell-surface molecules were then stained in HBSS with 3% FBS, followed by fixation. For intracellular staining of transcription factors, cells were fixed and permeabilized with a Foxp3 staining buffer set (eBioscience). For intracellular staining of cytokines, cells were stimulated ex vivo by 50 ng/ml PMA and 500 ng/ml ionomycin for 4 hr and 10 ng/ml IL-23 for 6-24 hr. Brefeldin A (2g/ml) was added 2 hr before cells were harvested for analysis. Then cells were fixed in 1% formyl saline and were permeabilized with 0.1% saponin buffer. Flow cytometry data were collected with Gallios (Beckman Coulter) instrument and the results were analyzed with FCS Express 6 software (De Novo Software).

Antibodies specific to mouse CD3(17A2, #11-0032-82), RORγt (B2D, #12-6981), IL-22 (IL22JOP, #17-7222-80) were purchased from eBioscience and CD90 (53-2.1, #140322) was purchased from Biolegend.

***C. rodentium* Infection**

C. rodentium strain DBS100 (ATCC 51459; American Type Culture Collection) was prepared by culturing in LB broth overnight and bacterial concentration was determined by measuring the optical density at 600 nm (OD600). Mice were gavaged with 10^{10} CFU in 200ulphosphate-buffered saline (PBS).

Quantitative real-time PCR

Total RNA was isolated with Trizol reagent (Invitrogen) and then reversed-transcribed with a Reverse Transcription System (Vazyme) following the manufacturer's protocol. The cDNA was amplified by an ABI 7500 Detection System using the AceQ qPCR SYBR Green Master Mix (Low ROX Premixed) (Vazyme) and the primers were showed below:

primer name	sequence (5'→3')
ELF4 RT F	CATCATAACAGACGGGACCTTG
ELF4 RT R	GCTGGGAGACTCCATATTGAGTA
HPRT1 RT F	CCTGGCGTCGTGATTAGTGA
HPRT1 RT R	CGAGCAAGACGTTCAGTCCT
Elf4 RT F	AACGTGTCATCCACTGAAGTC
Elf4 RT R	TCAGGGGTAGAGAGCAGGAAG
Hprt1 RT F	TCAGTCAACGGGGGACATAAA
Hprt1 RT R	GGGGCTGTACTGCTTAACCAG
Muc2 RT F	TCCTGACCAAGAGCGAACAC

Muc2 RT R	GGGTAGGGTCACCTCCATCT
Muc3 RT F	GCTGGCTTTCATCCTCCACT
Muc3 RT R	CTGTTTTCCCCGTCTGTGGT
Muc13 RT F	TCAACCCTTCCCACCATCCT
Muc13 RT R	TGAGATGAACTACCCACGGTC
Reg3b RT F	ATGGCTCCTACTGCTATGCC
Reg3b RT R	GTGTCCTCCAGGCCTCTT
Reg3g RT F	CAGACAAGATGCTTCCCCGT
Reg3g RT R	GTTCATAGCCCAGTGTCGGG
Nabp1 RT F	TGAATTACCGCTTCCTGACCC
Nabp1 RT R	TTGGTCACTCGTCCTATCTCCA
Nbn RT F	CCAAGGGCTCGTATTCTACTCTG
Nbn RT R	CACTCACCTTGTCATGGTATCAG
Fbxo18 RT F	GCCATCGTTTGTTCCCATCG
Fbxo18 RT R	GCCCATAGTATGAGTCAGGCAA
Ints3 RT F	TCCAGCGCCAGTACCTCTC
Ints3 RT R	GTTGGACGTGCATGTTGTCA
H2ax RT F	CGGTGGGCTTGAAGGTTAGT
H2ax RT R	GCGACAGGGTCAACTGGTATG
Taok3 RT F	TTGCATGAAATTGGACATGGGA
Taok3 RT R	CGATGGTGTTAGGATGCTTCAG
Il-22 RT F	GACCAAACTCAGCAATCAGCTC

Il-22 RT R	TACAGACGCAAGCATTTCTCAG
NBN-RT-F	CACTCACCTTGTCATGGTATCAG
NBN-RT-R	CTGCTTCTTGGACTCAACTGC
FBXO18-RT-F	CACTTGTGGAGGGAGATCATCA
FBXO18-RT-R	TGGCTGTGTATCGTATGAGGTT
TAOK3-RT-F	AACAGAGCCAGGTCAGGTAAA
TAOK3-RT-R	TTCCGTTCCGCCAATTCAATA
INTS3-RT-F	GAAGTGTTACCGGGACTTAGC
INTS3-RT-R	CCAACTGAGTACGGCAGGTAT
NABP1-RT-F1	CGCGCCTGTCCCAATATGAA
NABP1-RT-R1	TTTGGTCACGCGTCCTATCT
H2AX RT F	GTGGTGCTTAGCCCAGGACT
H2AX RT R	CCAGCGCAGACCTATGAATGAA

Whole genome RNA sequencing

Wild type control and Elf4 deficient mice were treated with 2% DSS, and the inflamed distal colons were collected at day 6. Total RNA was isolated with Trizol reagent (Invitrogen). The transcriptome library for sequencing was generated using VAHTSTM mRNA-seq v2Library Prep Kit for Illumina® (Vazyme Biotech Co.,Ltd, Nanjing, China) following the manufacturer's recommendations. The libraries were then sequenced on Illumina Hiseq X Ten platform using (2×150bp) paired-end module. Raw reads were obtained by base calling using CASAVA (http://www. illumina.com/ support/documentation.ilmn). Then, raw reads in a fastq format were first processed

using in-house perl scripts. Clean reads were obtained by removing reads with adapters, reads in which unknown bases were more than 5% and low quality reads (the percentage of low quality bases was over 50% in a read, we defined the low quality base to be the base whose sequencing quality was no more than 10). At the same time, Q20, Q30, GC content of the clean data were calculated (Vazyme Biotech Co.,Ltd, Nanjing, China). The primary data can be accessed at Gene Expression Omnibus with the identifier "GSE121305".

Lentivirus shRNA vector mediated gene knockdown

After transfecting the lentiviral vector, psPAX2 and pMD2.G into HEK293T cells for 48 h, the supernatants were collected to infect SW480 cells. Puromycin was used for selection of positive cells.

CRISPR-mediated ELF4 knockout cell line and ELF4 partial promoter region knockout SW480 cells

The sequence (GAGTTGGACGACGTTCACAA) of the human ELF4 genome was selected as the target. Oligos were ligased into the BsmB1 restriction site of the inducible lentiviral vector (lentiGuide-Puro). Lentivirus particles were produced by co-transfected HEK293 cells with guide RNA plasmids (2.4 ug), packaging plasmids pCMV-VSV-G (800ng, AddGene 8454) and psPAX2 (800ng, AddGene 12260). The medium was changed to fresh DMEM containing 20% FBS at 24 hours post transfection and viral supernatant was collected at 48-72 hours. Then, a total of 1×10^5 SW480 or NCM460 cells were infected with viral supernatant supplemented with 8

ug/ml polybrene and incubated for 48 hours. Possible knockout cells were screened by puromycin (4 μg/ml for NCM460 cells and 10μg/ml for SW480 cells) and each monoclone was confirmed by sequencing and western blot. Cells were negative for mycoplasma.

For ELF4 partial promoter region knockout SW480 cells, the sequence between (GTGCCTGAGTGGCTTTCAAG) and (GTTCCAAAATTGTATCCTCT) of the human ELF4 promoter region was selected as the target.

Induction of colitis and Colorectal Cancer

For induction of chronic colitis(Whittem et al., 2010), mice were treated with 3 cycles of DSS induction. 1 cycle was defined as 1.5% DSS for 5-7 days followed by 14 days resting (regular water drinking).

For induction of CAC(Thaker et al., 2012), a single intraperitoneal injection with 10 mg/kg of AOM was followed by three seven-day cycles of 1.5% DSS over a 10 week period.

For induction of acute colitis(Whittem et al., 2010), mice were treated with 3% DSS for 5-7 days.

Comet tail assay

SW480 and NCM460 cells were seeded on 6-well plates at a concentration of 5×10^6 /ml. Then cells were treated with H_2O_2 at 2mM for SW480 and 300uM for NCM460

for indicated time. Lysis, electrophoresis and quantification of DNA breaks were as described(Fang et al., 2015).

Histopathological analysis

Formalin-preserved colon sections were processed and embedded in paraffin by standard techniques. Longitudinal sections of 5 mm thick were stained with hematoxylin and eosin (H&E). Colitis scoring was as previously described(Zaki et al., 2011). Briefly, Inflammation extent, ulceration and hyperplasia of the mucosa were chosen as principal parameters. Colon tumor scoring was described(Meira et al., 2008). Inflammation, dysplasia/neoplasia and area of dysplasia/neoplasia were chosen as principal parameters.

Bisulfite sequencing and mass spectrometry

Bisulfite sequencing was used to generate DNA-methylation maps with single-base resolution. The method is based on the selective deamination of cytosine to uracil (and subsequent conversion to thymine via PCR), whereas 5-methylcytosine residues remain unchanged(Wang et al., 2014). Genomic DNA from tissues and cells were bisulfite-converted with the EpiTect Bisulfite Kit (QIAGEN) according to the manufacturer's instruction, followed by PCR designed to amplify the ELF4 gene promoter. Quantitative methylation analysis was performed by Sequenom's MassARRAY platform9. The methylation level on individual CpG site refers to the percentage of methylated CpG dinucleotides in the settings of total DNA (1 refers to 100%), which is generated by the EpiTYPER software v1.0 (Sequenom).

hELF4-methylation-F	**aggaagagagGTGTTTGAGTGGTTTTTAAGTGGG**
hELF4-methylation-R	cagtaatacgactcactatagggagaaggctAAACTCCTAAAATATAC AAACCCCAA
mElf4-methylation-F	aggaagagagAGTGTATGTTTGGTATTGTGGAGTG
mElf4-methylation-R	cagtaatacgactcactatagggagaaggctACAAAAAAAACCTTACC AAAAACCC

Montmorillonite powder treatment

Montmorillonite powder was dissolved and diluted in sterile water. The gavage dose was 1g/kg and performed every other day. The intervention started at day 3 or day 4 during the course of colitis induction by DSS. For tumor prevention experiment, each cycle of DSS treatment was combined with montmorillonite gavage as mentioned above.

Statistical analysis

Samples were compared using two-tailed, unpaired Student's *t*-test, unless otherwise stated with GraphPad Prism 7.00. Error bars were represented by SEM.

References

Fang, K., Bruce, M., Pattillo, C.B., Zhang, S., Stone, R., 2nd, Clifford, J., and Kevil, C.G. (2011). Temporal genomewide expression profiling of DSS colitis reveals novel inflammatory and angiogenesis genes similar to ulcerative colitis. Physiol Genomics *43*, 43-56.

Fang, L., Neutzner, A., Turtschi, S., Flammer, J., and Mozaffarieh, M. (2015). Comet assay as an indirect

measure of systemic oxidative stress. J Vis Exp, e52763.
Maluach, A.M., Misquitta, K.A., Prevot, T.D., Fee, C., Sibille, E., Banasr, M., and Andreazza, A.C. (2017). Increased Neuronal DNA/RNA Oxidation in the Frontal Cortex of Mice Subjected to Unpredictable Chronic Mild Stress. Chronic Stress (Thousand Oaks) *1*.
Meira, L.B., Bugni, J.M., Green, S.L., Lee, C.W., Pang, B., Borenshtein, D., Rickman, B.H., Rogers, A.B., Moroski-Erkul, C.A., McFaline, J.L.*, et al.* (2008). DNA damage induced by chronic inflammation contributes to colon carcinogenesis in mice. The Journal of clinical investigation *118*, 2516-2525.
Olsen, J., Gerds, T.A., Seidelin, J.B., Csillag, C., Bjerrum, J.T., Troelsen, J.T., and Nielsen, O.H. (2009). Diagnosis of ulcerative colitis before onset of inflammation by multivariate modeling of genome-wide gene expression data. Inflammatory bowel diseases *15*, 1032-1038.
Planell, N., Lozano, J.J., Mora-Buch, R., Masamunt, M.C., Jimeno, M., Ordas, I., Esteller, M., Ricart, E., Pique, J.M., Panes, J.*, et al.* (2013). Transcriptional analysis of the intestinal mucosa of patients with ulcerative colitis in remission reveals lasting epithelial cell alterations. Gut *62*, 967-976.
Qiu, J., Heller, J.J., Guo, X., Chen, Z.M., Fish, K., Fu, Y.X., and Zhou, L. (2012). The aryl hydrocarbon receptor regulates gut immunity through modulation of innate lymphoid cells. Immunity *36*, 92-104.
Thaker, A.I., Shaker, A., Rao, M.S., and Ciorba, M.A. (2012). Modeling colitis-associated cancer with azoxymethane (AOM) and dextran sulfate sodium (DSS). J Vis Exp.
Wang, Y., Gu, X., Zhang, G., Wang, L., Wang, T., Zhao, Y., Zhang, X., Zhou, Y., Kadin, M., and Tu, P. (2014). SATB1 overexpression promotes malignant T-cell proliferation in cutaneous CD30+ lymphoproliferative disease by repressing p21. Blood *123*, 3452-3461.
Whittem, C.G., Williams, A.D., and Williams, C.S. (2010). Murine Colitis modeling using Dextran Sulfate Sodium (DSS). J Vis Exp.
You, F., Wang, P., Yang, L., Yang, G., Zhao, Y.O., Qian, F., Walker, W., Sutton, R., Montgomery, R., Lin, R.*, et al.* (2013). ELF4 is critical for induction of type I interferon and the host antiviral response. Nature immunology *14*, 1237-1246.
Zaki, M.H., Vogel, P., Malireddi, R.K., Body-Malapel, M., Anand, P.K., Bertin, J., Green, D.R., Lamkanfi, M., and Kanneganti, T.D. (2011). The NOD-like receptor NLRP12 attenuates colon inflammation and tumorigenesis. Cancer cell *20*, 649-660.